GEOLOGICA BELGICA (2018) 21/1-2: 1-17

Geochemistry and origin of Carboniferous (Mississippian; Viséan) bentonites in the Namur-Dinant Basin, Belgium: evidence for a Variscan volcanic source

Michael A. POINTON[1,2*], David M. CHEW[1], Bernard DELCAMBRE[3], George D. SEVASTOPULO[1]

[1]*Department of Geology, School of Natural Sciences, Trinity College Dublin, College Green, Dublin 2, Ireland; pointonm@tcd.ie.*
[2]*Present address: CASP, West Building, Madingley Rise, Madingley Road, Cambridge, CB3 0UD, United Kingdom.*
[3]*Earth and Life Institute, Université Catholique de Louvain, Place Louis Pasteur 3, B-1348, Louvain-la-Neuve, Belgium.*
** corresponding author*

ABSTRACT. Several thin clay-rich horizons occur interbedded with Mississippian (Viséan) limestones in the Namur-Dinant Basin, southern Belgium. These have been interpreted as diagenetically altered volcanic ash layers (bentonites). Whole-rock geochemical analysis of several bentonites was undertaken to provide insight into their original magmatic composition. Ratios of several trace elements that are considered to be immobile during diagenetic alteration and indicators of petrogenetic processes suggest that most of the bentonites were originally trachyandesitic to trachytic ashes. Furthermore, the coarse grain size of euhedral zircon phenocrysts (up to 400 µm in length) suggests a proximal volcanic source. Zircon U–Pb isotopic ages and whole-rock geochemical data from these bentonites were compared with literature data from volcanic and intrusive rocks in adjacent areas, and suggest that the bentonites were sourced from volcanoes within the Variscan orogenic belt.

KEYWORDS: altered volcanic ash, cinerite, whole-rock geochemistry, trace element geochemistry, X-ray diffraction analysis.

1. Introduction

Several clay-rich horizons interbedded with Mississippian (Viséan) limestones in the Namur-Dinant Basin (NDB), Belgium, are interpreted to be diagenetically altered volcanic ash layers based on their lateral continuity, clay mineralogy and heavy mineral assemblages (e.g. Thorez & Pirlet, 1979; Delcambre, 1989, 1996). Whilst several aspects of these clay horizons have been studied in detail, their original (unaltered) volcanic composition and the location(s) of the source volcanoes are not well constrained. The whole-rock geochemistry of altered volcanic rocks such as bentonites and tonsteins has been employed in several other studies to gain information about the composition of the original (unaltered) ash layers and ultimately the magma from which they were derived (e.g. Spears & Kanaris-Sotiriou, 1979; Merriman & Roberts, 1990; Huff et al., 1993; Christidis et al., 1995). The major elements, which are routinely used to classify fresh or slightly altered volcanic rocks, are of limited use when classifying extensively altered volcanic rocks because several elements, including K and Na, are known to be mobile during weathering and diagenesis (Winchester & Floyd, 1977; Floyd & Winchester, 1978; Zielinski, 1982; Christidis, 1998). Instead, the classification of altered volcanic rocks relies on trace elements including Ti, the high-field-strength elements (HFSE) Hf, Nb, Ta, Zr and the rare-earth elements, which are generally considered to be immobile during most upper crustal processes and are also indicators of petrogenetic processes (Floyd & Winchester, 1978; Huff et al., 1993). There are potential pitfalls associated with using whole-rock geochemistry; for example, aeolian fractionation of volcanic particles during transportation can modify the bulk composition of a distal ash layer (e.g. Huff et al., 1993). Likewise, post-depositional processes such as sedimentary reworking can modify whole-rock geochemistry (e.g. Clayton et al., 1996), although detrital additions can commonly be detected by studying the bulk mineralogy and heavy mineral assemblages of bentonites. As part of a wider study, several bentonites in the NDB were sampled for whole-rock geochemical analysis to provide insight into their volcanic source(s). Whole-rock powder X-ray diffraction (XRD) analyses were also undertaken to provide mineralogical constraints on the bentonites and to help explain the geochemical variations observed between different bentonite samples.

2. Geological Setting

The Namur-Dinant Basin of southern Belgium lies within the northwestern part of the Rhenohercynian fold belt (Poty et al., 2001). The basin was initiated during Devonian times as two separate basins, the Namur Basin to the north and the Dinant Basin to the south, which were connected by early Carboniferous times (McCann et al., 2006). The basin is dissected by the Midi Fault, a major E-W trending Variscan thrust fault (Fig. 1), which separates the Brabant Para-autochthon to the north from the southern Ardenne Allochthon (Fig. 1; Poty et al., 2001). Mississippian carbonate strata crop out on both sides of the Midi Fault and are inferred to have been deposited within the same sedimentary basin (Poty et al., 2001). Seven sedimentation areas (or depocentres) have been recognised within the basin (Fig. 1; Poty, 2016). These are distinguished by different sedimentation patterns during Tournaisian and early Viséan times, when both differential subsidence and the development of Waulsortian mud mound facies generated topographic irregularities (Hance et al., 2006). Later in the Viséan, sedimentation within the basin became more uniform and lithostratigraphic units can be traced between the different sedimentation areas (Fig. 2). The basin is inferred to have evolved from a south-facing homoclinal ramp during early Tournaisian times to a rimmed shelf during early Viséan times and then into an aggrading carbonate platform during middle to late Viséan times (Hance et al., 2002).

Early Livian strata of the Lives Formation are well exposed in several areas of the basin (Fig. 2). Late Livian rocks, whilst also well exposed, are brecciated across a wide area of the basin (Grande Brèche Viséenne; Fig. 2). Brecciation is thought to be related to the dissolution of evaporite horizons and/or an early phase of Variscan shortening (Poty et al., 2001 and references therein). Unbrecciated late Livian strata are restricted mostly to the northern Namur sedimentation area (NSA; Poty & Hance, 2006a; Fig. 2). The Warnantian stratigraphic record is incomplete within the basin; the most complete stratigraphic records are found in the Dinant and Condroz sedimentation areas (DSA and CSA respectively), where only latest Warnantian strata are missing (Fig. 2; Poty & Hance, 2006b). To the north and east within the basin, the amount of stratigraphic omission increases and extends stratigraphically downwards; in the northern NSA, Namurian siliciclastic strata rest upon latest Livian to earliest Warnantian strata (Hance et al., 2002; Poty & Hance, 2006b; Fig. 2). The Livian and Early Warnantian stratigraphy comprises alternations of subtidal bioclastic limestones overlain by intertidal to supratidal micrites and stomatolitic boundstones which have been interpreted as shallowing upwards parasequences (Pirlet, 1963; Chevalier & Aretz, 2005; Poty & Hance, 2006a, 2006b). Using U–Pb zircon chemical abrasion isotope dilution thermal ionisation mass spectrometry (CA-ID-TIMS) dates from bentonites W8 and W13 (Fig. 2), Pointon et al. (2014) determined that the intervening Early Warnantian parasequences have an average

http://dx.doi.org/10.20341/gb.2017.011

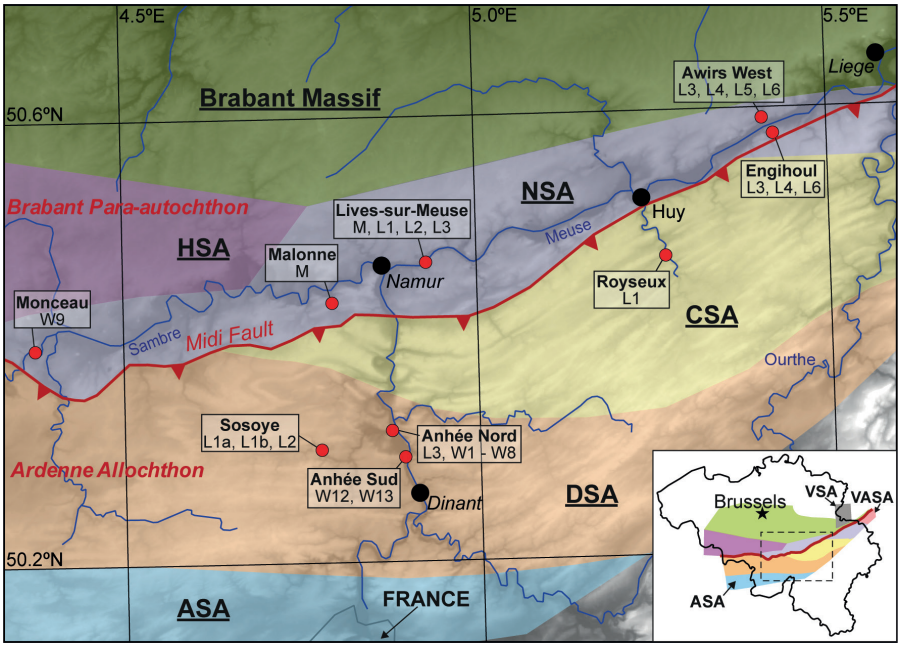

Figure 1. Map showing sampling localities. Sedimentation areas are redrawn from Poty (2016; not palinspastic). ASA = southern Avesnois sedimentation area (see inset map), CSA = Condroz sedimentation area, DSA = Dinant sedimentation area, HSA = Hainaut sedimentation area, NSA = Namur sedimentation area, VASA = Vesdre – Achen sedimentation area (see inset map); VSA = Visé-Maastricht sedimentation area (see inset map). The rectangle in the inset map shows the area of Belgium covered by the main diagram. The Midi Fault separates the Brabant Para-autochthon from the Ardenne Allochthon. The topographic base map is after Jarvis et al. (2008).

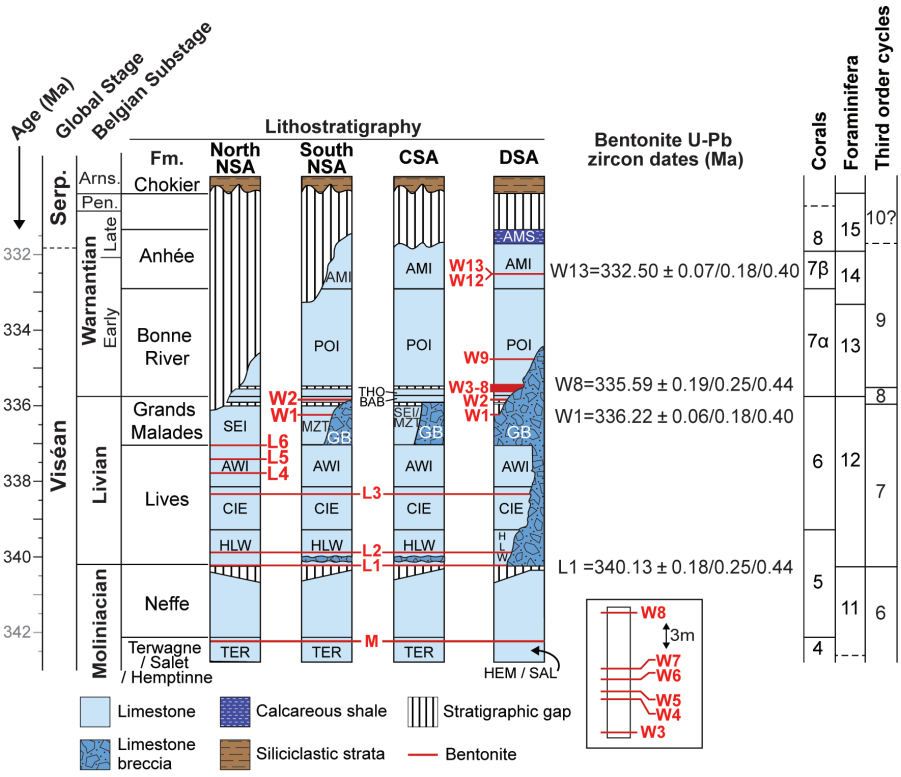

Figure 2. Lithostratigraphic framework for the middle to late Viséan of the Namur-Dinant Basin, redrawn and modified from Devuyst et al. (2006), Poty & Hance (2006a, 2006b) and Poty (2016) so that it is scaled by U–Pb isotopic age. Ages shown in black are interpolated from the bentonite U–Pb zircon dates whereas ages shown in grey are extrapolated; interpolation / extrapolation was done using the OXCAL program (P_Sequence routine, input parameters: 1,5,U(-5,5); Bronk Ramsey, 2008; Bronk Ramsey & Lee, 2013). Bentonite U–Pb dates are from Pointon et al. (2014) except that of bentonite L1 (Banc d'or de Bachant) which is from Pointon (2012). U–Pb zircon date uncertainties are given in the ± X/Y/Z notation of Schoene et al. (2006) where X is the internal error, Y is the internal error plus tracer calibration uncertainties and Z is the internal error plus tracer and U decay constant uncertainties (all 2σ / 95% confidence). Mississippian Foraminifera biozones and Rugose Coral biozones are drawn following Poty et al. (2006). Third order sequence stratigraphic cycles are drawn following Hance et al. (2002) and Poty & Hance (2006b). AMI and AMS, Lower and Upper members of the Anhée Formation respectively; Arns. = Arnsbergian; AWI = Awirs Member; BAB = Bay Bonnet Member; CIE = Corphalie Member; Fm = Formation; GB = Grande Brèche Viséenne; HEM = Hemptinne Formation; HLW = Haut-le-Wastia Member; MZT = Maizeret Member; Pen. = Pendleian; POI = Poilvache Member; SAL = Salet Formation; SEI = Seilles Member; Serp. = Serpukhovian; TER = Terwagne Formation; THO = Thon-Samson Member. The base of the Serpukhovian Global Stage has not yet been ratified but will probably be chosen to coincide with the first appearance datum (FAD) of the conodont *Lochriea ziegleri* (Sevastopulo & Barham, 2014). *Lochriea ziegleri* has not been reported from the Namur-Dinant Basin; however, the boundary can be tentatively correlated to a level within the uppermost Lower Member of the Anhée Formation using foraminifera (Conil et al., 1991; Poty et al., 2006) and ammonoids (Pirlet, 1968; Paproth et al., 1983) in conjunction with the correlations between the FAD of *Lochriea ziegleri* and NW European ammonoid / foraminifera biozones suggested by Barham et al. (2015).

periodicity of 101 – 129 kyr / cycle and are consistent with the *c.* 100 kyr Milankovitch cycle, which is the dominant Milankovitch frequency recognised from recent Pleistocene glacial records (e.g. Imbrie et al., 1993).

3. Viséan bentonites

Several clay-rich horizons ranging in thickness from *c.* 1 to 30 cm occur interbedded with Moliniacian to Warnantian (Viséan) limestones and have been interpreted to be diagenetically altered volcanic ash layers (e.g. Thorez & Pirlet, 1979; Delcambre, 1989). The horizons have been termed cinerites by some Belgian workers (e.g. Delcambre, 1989) and K-bentonites by others (e.g. Thorez & Pirlet, 1979). Their mineralogy has been studied previously (Thorez & Pirlet, 1979; Delcambre, 1989; Anceau, 1992, 1996) and is only summarised here. The bentonites comprise mostly polymineralic clays, including mixed-layer clays (illite/

smectite, illite/vermiculite, illite/chlorite), illite, kaolinite and/or Al-rich chlorites (Thorez & Pirlet, 1979; Anceau, 1992, 1996). The clay mineralogy varies laterally and vertically, both within a single bentonite and between different bentonites (Thorez & Pirlet, 1979; Anceau, 1992, 1996). Thorez & Pirlet (1979) noted that the clay mineral assemblages are consistent with the early diagenetic alteration of volcanic ash in a marine environment, although some modification during burial diagenesis cannot be excluded as Mississippian strata within the basin have experienced temperatures of up to *c*. 250 °C based on illite crystallinity and conodont alteration indices (Helsen & Kønigshof, 1994; Han et al., 2000).

Aside from the volumetrically dominant clay minerals, the bentonites also contain trace amounts of coarser-grained volcanic phenocrysts including splintery quartz, biotite (in varying stages of alteration), euhedral apatite and zircon, and pseudomorphs after feldspar (Thorez & Pirlet, 1979; Delcambre, 1989, 1996; Pointon et al., 2014). Primary bentonites, i.e. those deposited from air-borne ash and altered *in situ*, have been shown to contain a restricted suite of heavy minerals comprising biotite, zircon, apatite and titanite (Weaver, 1963). The similarly restricted heavy mineral assemblages from most of the NDB bentonites, coupled with the idiomorphic shape of the zircon and apatite grains, strongly supports that the NDB bentonites are largely of primary origin. Many of the NDB bentonites occur interbedded with micritic limestones. The relatively low-energy depositional environment, with minimal clastic input, likely helped to preserve the NBD bentonites and their primary (volcanic) mineralogy.

Zircons separated from three late Livian to Early Warnantian bentonite horizons have yielded precise U–Pb CA-ID-TIMS dates, which were interpreted to approximate the timing of eruption (Fig. 2; Pointon et al., 2014). Additionally, unpublished U–Pb zircon CA-ID-TIMS data from bentonite L1 (also known as the Banc d'or de Bachant) at Lives-sur-Meuse, yielded a weighted mean $^{206}Pb/^{238}U$ date of 340.13 ± 0.18 Ma (MSWD = 0.96; n = 3; Pointon, 2012; all U–Pb isotopic dates are quoted at the 2σ / 95% confidence level), and provides an upper age limit for the majority of the bentonites studied here (Fig. 2). There are presently no absolute age constraints from bentonite M and biostratigraphical control is poor due to the development of widespread restricted, peritidal facies in the CSA and NSA during Moliniacian times (Devuyst et al., 2006; Poty et al., 2006).

Several bentonites have been correlated between different localities within the NDB using zircon typology (Delcambre, 1989, 1996). Furthermore, the uniformity of the Livian and Warnantian stratigraphy across a wide area of the basin (e.g. Hance et al., 2006) permits reliable lithostratigraphic correlation of several bentonite beds across a large area of the basin.

4. Materials and methods

4.1. Samples

Eighteen Moliniacian to Warnantian bentonites were sampled for whole-rock geochemistry and whole-rock X-ray diffraction (XRD) analysis (Figs 1 & 2). Additionally, whole-rock geochemistry was undertaken on two limestone samples from the Corphalie Member of the Lives Formation (Fig. 2) at Lives-sur-Meuse (samples MAP02-28 and MAP03-02; from *c*. 1.2 and 7 m below bentonite L3 respectively) and a limestone sample from the Lower Member of the Anhée Formation (Fig. 2) at Anhée Sud (sample MAP07-41; from *c*. 4 m above the base of the formation). The field relationships of the majority of the bentonite horizons investigated in this study have been described previously by Delcambre (1989, 1996) and Pointon et al. (2014). Three previously undescribed bentonites within the Awirs Member, Lives Formation, have been observed at Awirs West and Engihoul quarries in the northern NSA (Figs 1 & 2). These horizons are herein named L4, L5 and L6 (Fig. 2) following the nomenclatural scheme established by Delcambre (1989, 1996). At the Awirs West locality, a weathered section in a now disused quarry, bentonite L4 comprises two visually distinctive layers (a lower orange plastic clay layer and an upper black poorly consolidated layer), bentonite L5 is orange-black, internally homogeneous and poorly consolidated, and bentonite L6 is orange, internally homogeneous and has a plastic, clay-like texture. The thickness of each bentonite varies laterally between *c*. 3 – 5 cm. In contrast, in the active Engihoul quarry, although the bentonites are of a similar thickness to those at Awirs West, the colours and textures differ as they are freshly exposed: bentonite L4 is a dark grey, homogeneous, well consolidated, fissile, silty claystone and bentonite L6 is a pale grey, homogeneous plastic clay layer. Bentonite L5 was not sampled.

Several bentonites were sampled from multiple localities within the basin (Fig. 1) to determine if significant lateral chemical and mineralogical variations are present. In the Livian stratotype section at Lives-sur-Meuse, bentonite L1, which is more widely known as the Banc d'or de Bachant, is represented by a single bentonite layer. However, towards the south and east of the basin (ASA, DSA; Fig. 1), at the same stratigraphic level, up to three bentonite layers separated by thin limestone horizons occur within an interval of <1m total thickness (Delcambre 1989, 1996). These closely-spaced bentonites are dominated by S18, S19, S23 and S24 prismatic zircon shapes, similar to bentonite L1 elsewhere within the basin (Delcambre 1989, 1996). Consequently, it has been suggested that these horizons coalesce towards the north and west of the basin where bentonite L1 is represented by only a single layer (e.g. at Lives-sur-Meuse; Delcambre 1989, 1996). In this study, the splitting of bentonite L1 was observed at Sosoye, where a lower *c*. 15 cm thick bentonite (L1a) and an upper *c*. 2 cm thick bentonite (L1b) occur separated by <1 m of limestone. At the other three sampling sites (Fig. 1) only a single bentonite L1 horizon was observed.

Samples were also collected from the base and top of three bentonite horizons (L4 and L6 from Awirs West quarry and W8 from Anhée Nord) to investigate for vertical geochemical stratification within the bentonite horizons. Bentonites L4 and L6 in Awirs West quarry have been described above. Bentonite W8 at Anhée Nord is *c*. 18 cm thick, red-brown, silicified and internally homogeneous.

4.2. Whole-rock geochemical analysis

Samples were crushed in a tungsten carbide jaw crusher to <3 mm grain size, dried at 105 °C overnight and then comminuted using a Retsch planetary ball mill equipped with a 50 ml agate grinding jar or a TEMA tungsten carbide ring-and-puck mill. The use of a tungsten carbide mill and jaw crusher can add trace quantities of tungsten and cobalt to samples (e.g. Buhrke et al., 1998), so tungsten concentrations are not discussed, while cobalt concentrations were not determined. Whole-rock geochemical analyses (major, trace and rare-earth elements) were determined from 6 – 8 g of sample at OMAC Laboratories (now ALS Loughrea), Ireland. Samples were analysed following their lithium borate fusion (BF ES/MS) protocol. Major elements were measured using inductively coupled plasma atomic emission spectroscopy (ICP-AES), whereas trace and rare-earth elements were determined using inductively coupled plasma mass spectrometry (ICP-MS). The accuracy of the analyses and the stability of the ICP machines were monitored by interspersing analyses of in-house standard materials between unknown sample analyses. Replicate analyses were undertaken every 10 unknown analyses, the reproducibility of which was better than 10% (2σ), except where analytes approached the limit-of-detection. Replicate analyses were averaged and these are used in the interpretation below. Analytes below the limit of detection are arbitrarily assigned a value of half the limit of detection in the figures; these are clearly labelled in Table 1 and predominantly affect the limestone analyses. Loss-on-ignition ranged from 8.03 to 32.84%, with the highest values recorded in samples that contain substantial carbonate (e.g. M from Malonne, L1b from Sosoye and L6 from Engihoul quarry).

Table 1. Whole-rock geochemistry data from Mississippian (Viséan) bentonites and limestones of the Namur-Dinant Basin.

Sample[1]	M	M	L1	L1	L1a	L1b	L2	L2	L3	L3	L3	L3
Locality[2]	L-s-M	Mal	L-s-M	Roy	Sos	Sos	L-s-M	Sos	AN	AW	Eng	L-s-M
SiO_2	44.02	15.72	46.86	42.81	52.00	27.30	45.28	51.71	42.74	47.71	45.90	40.14
Al_2O_3	22.88	7.93	28.92	26.93	25.46	15.70	29.38	23.16	17.11	27.07	15.89	27.50
CaO	5.44	38.33	0.42	0.90	0.81	25.29	1.20	2.05	12.29	2.68	11.35	6.26
Cr_2O_3	0.022	0.007	0.023	0.037	0.010	0.007	0.013	0.005	0.002	0.00	0.00	0.003
Fe_2O_3	5.47	2.61	3.93	9.27	3.19	2.16	6.69	4.67	2.21	2.40	2.16	4.21
K_2O	6.23	1.88	8.20	5.70	6.46	4.08	6.66	4.29	3.54	4.18	3.63	2.60
MgO	2.26	1.34	1.99	3.15	2.76	1.87	1.01	3.87	3.57	2.98	3.69	1.46
MnO	0.005	0.027	0.004	0.019	0.001	0.010	0.038	0.004	0.019	0.00	0.02	0.015
Na_2O	0.18	0.10	0.60	0.14	0.15	0.11	0.30	0.16	0.07	0.06	0.17	0.61
P_2O_5	0.03	0.04	0.08	0.03	0.03	0.02	0.49	0.28	0.09	0.16	0.10	0.21
TiO_2	1.20	0.35	1.09	0.88	0.68	0.43	0.77	0.47	0.28	0.40	0.26	0.45
LOI[3]	11.86	32.84	8.03	11.20	8.58	24.17	9.02	10.17	15.07	12.63	16.19	15.26
Ba	589.7	159.4	184.8	94.5	325.0	228.1	86.6	87.3	84.6	103.4	220.4	53.0
Ce	49.9	40.1	51.5	45.6	51.2	25.3	49.7	29.1	49.8	57.1	72.6	123.5
Dy	4.3	2.5	4.2	4.4	3.6	3.2	3.7	1.8	2.5	3.1	3.3	4.1
Er	3.0	1.5	2.7	3.2	2.1	2.0	2.2	1.0	1.2	1.5	1.4	2.0
Eu	0.6	0.5	0.5	0.5	0.7	0.4	0.5	0.2	0.2	0.3	0.4	0.4
Ga	23.3	10.0	31.4	22.2	42.4	25.6	8.6	20.7	11.6	26.8	18.3	16.3
Gd	3.3	2.7	3.2	3.2	3.9	2.4	4.4	2.2	3.0	3.7	4.5	5.4
Hf	16	4	14	11	11	6	13	8	6	11	6	13
Ho	0.9	0.5	0.9	1.0	0.7	0.7	0.7	0.4	0.4	0.5	0.6	0.7
La	23.9	21.7	26.9	25.6	26.6	13.0	18.7	10.0	17.0	19.5	28.0	44.9
Lu	0.5	0.2	0.4	0.5	0.3	0.3	0.3	0.2	0.2	0.2	0.2	0.3
Nb	55.4	19.7	63.1	43.0	40.4	23.6	18.8	15.1	15.2	24.0	15.3	22.3
Nd	18.3	16.4	15.8	18.9	21.3	11.7	22.9	14.0	18.6	23.2	28.2	41.4
Pr	5.2	4.8	5.0	5.5	6.4	3.3	5.8	3.4	5.4	6.5	7.9	12.2
Rb	295.0	99.4	212.4	129.4	402.9	239.9	164.6	114.6	88.6	118.6	116.2	76.7
Sc	17	7	21	25	16	9	8	7	6	7	6	9
Sm	3.8	3.0	3.6	3.3	4.6	2.7	4.9	3.1	4.0	4.7	6.0	7.0
Sn	4	3	7	12	7	6	5	6	3	8	5	10
Sr	222.7	605.3	67.1	40.3	69.2	279.8	26.9	26.5	149.0	40.1	96.4	115.3
Ta	3.6	1.3	3.7	2.7	3.2	1.8	3.6	2.8	2.1	3.6	2.1	3.3
Tb	0.6	0.4	0.6	0.6	0.6	0.5	0.6	0.3	0.5	0.6	0.6	0.8
Th	22.2	6.4	34.0	33.9	33.6	10.7	50.1	54.6	36.6	67.5	34.0	65.4
Tm	0.5	0.2	0.4	0.5	0.3	0.3	0.3	0.1	0.2	0.2	0.2	0.3
U	32.4	8.4	32.4	18.0	8.2	7.0	16.3	4.3	7.4	8.4	9.1	10.1
V	113.6	84.1	167.3	204.0	55.9	45.5	165.3	64.9	28.6	25.9	20.8	33.3
W	3.5	2.5	1.8	3.6	3.4	3.7	22.3	1.1	0.8	0.5	0.7	1.7
Y	23.8	14.9	24.4	34.6	19.9	17.5	23.5	10.2	10.2	12.9	12.1	16.5
Yb	3.3	1.5	3.1	3.5	2.2	2.1	2.1	1.0	1.1	1.2	1.1	1.8
Zr	611	142	524	414	429	220	401	244	189	315	190	375
Eu/Eu*[4]	0.53	0.50	0.50	0.47	0.48	0.51	0.34	0.27	0.19	0.19	0.22	0.20
ΣREE	118.0	96.1	118.8	116.4	124.6	67.8	117.0	66.8	104.0	122.2	154.9	244.6

Sample[1]	L4 (base)	L4 (top)[#]	L4	L5	L6 (base)	L6 (top)	L6	W1	W2	W3	W4	W5
Locality[2]	AW	AW	Eng	AW	AW	AW	Eng	AN	AN	AN	AN	AN
SiO_2	45.15	44.97	48.58	44.45	48.93	46.95	20.59	42.87	51.08	47.96	50.38	42.33
Al_2O_3	28.66	29.36	22.81	31.42	28.34	30.55	10.25	20.89	27.34	20.85	23.52	20.17
CaO	2.16	1.24	4.63	1.48	1.09	1.29	32.32	9.23	1.03	7.23	2.66	11.16
Cr_2O_3	0.002	0.005	0.003	<0.001	<0.001	0.002	0.001	0.002	0.001	0.002	<0.001	0.002
Fe_2O_3	3.08	4.35	2.79	2.57	2.01	2.65	3.64	3.09	3.42	3.31	3.09	3.10
K_2O	4.85	4.07	5.30	2.92	5.31	3.63	2.23	2.27	5.51	3.56	2.85	3.01
MgO	1.68	1.77	2.33	1.19	2.33	1.68	1.12	5.34	2.86	3.00	5.08	3.28
MnO	0.006	0.008	0.009	0.004	0.001	0.002	0.019	0.026	0.015	0.159	0.105	0.038
Na_2O	0.18	0.18	0.13	0.15	0.10	0.10	0.07	0.09	0.17	0.10	0.13	0.15
P_2O_5	0.06	0.08	0.03	0.13	0.15	0.09	0.04	0.17	0.15	0.17	0.10	0.19
TiO_2	0.26	0.33	0.25	0.36	0.38	0.36	0.65	0.39	0.51	0.27	0.23	0.41
LOI[3]	12.86	14.20	12.31	13.86	12.44	13.33	25.70	15.81	9.37	14.48	11.20	16.67
Ba	90.9	105.3	5764.4	55.2	82.4	66.2	631.8	123.3	94.2	353.6	142.5	84.5
Ce	15.3	35.7	26.7	9.2	15.2	12.0	118.2	26.9	14.9	13.6	7.9	18.8
Dy	3.0	3.0	2.2	1.5	3.9	3.7	8.0	1.6	1.5	1.2	1.6	2.6
Er	2.2	2.2	1.5	1.1	2.5	2.3	4.5	1.0	1.0	0.8	0.8	1.4
Eu	0.1	0.1	0.3	0.1	0.2	0.2	2.2	0.3	0.2	0.2	0.3	0.3
Ga	21.1	21.4	22.5	15.7	23.7	20.0	19.6	13.2	20.5	14.4	12.8	13.4
Gd	1.7	1.9	1.6	1.3	2.7	2.4	8.2	1.6	1.2	1.1	1.5	2.2
Hf	10	9	6	12	12	10	15	5	7	7	9	7
Ho	0.6	0.7	0.5	0.3	0.8	0.7	1.6	0.3	0.3	0.2	0.3	0.5
La	6.0	17.0	12.8	3.4	5.0	3.8	51.1	11.8	7.0	5.5	2.8	7.5
Lu	0.4	0.4	0.3	0.2	0.5	0.4	0.6	0.2	0.2	0.1	0.1	0.2
Nb	16.8	22.8	20.8	22.6	24.5	24.4	135.8	12.9	14.1	20.1	18.0	21.6
Nd	5.4	8.9	8.1	4.9	9.3	6.9	46.9	9.8	6.0	5.6	3.9	9.4
Pr	1.6	3.2	2.5	1.1	2.1	1.7	13.1	2.8	1.7	1.4	0.9	2.2
Rb	119.6	113.3	160.4	76.1	136.6	118.6	69.2	58.7	141.7	79.5	71.3	72.0
Sc	10	10	8	9	8	8	6	6	6	6	4	10
Sm	1.7	2.0	1.7	1.5	2.9	2.6	9.8	2.0	1.3	1.3	1.5	2.4
Sn	3	4	4	3	8	6	3	2	1	2	1	2
Sr	22.1	29.7	88.3	22.7	11.8	9.8	155.7	126.4	48.3	137.6	25.6	68.1
Ta	3.3	3.5	2.0	3.0	3.5	3.5	8.5	1.8	2.0	2.7	3.6	2.1
Tb	0.4	0.4	0.3	0.3	0.6	0.5	1.4	0.3	0.2	0.2	0.2	0.4
Th	31.0	50.2	44.7	38.9	39.9	54.7	15.3	21.9	26.7	37.5	50.3	25.3
Tm	0.4	0.4	0.3	0.2	0.4	0.4	0.7	0.2	0.2	0.1	0.1	0.2
U	11.2	18.2	7.7	5.4	6.9	7.4	14.5	18.4	22.4	6.7	11.7	26.8
V	19.7	65.3	18.0	26.2	42.0	41.4	51.6	68.6	79.0	49.4	66.7	113.8
W	2.3	17.9	0.8	0.7	2.5	0.7	1.4	1.3	22.8	0.9	1.8	1.5
Y	14.8	14.7	11.7	8.2	19.2	17.4	42.9	8.7	8.4	7.9	9.1	14.5
Yb	3.0	2.9	1.8	1.2	2.8	2.5	4.4	1.1	1.2	0.8	0.8	1.2
Zr	248	243	177	372	369	299	631	168	225	189	247	215
Eu/Eu*[4]	0.22	0.19	0.62	0.30	0.20	0.23	0.73	0.53	0.50	0.49	0.51	0.41
ΣREE	41.9	78.8	60.8	26.4	48.9	40.1	270.8	59.9	36.8	32.3	22.8	49.4

Sample[1]	W6	W7+	W8 (base)	W8 (top)	W9	W12#	W13	MAP07-41 (BL)	MAP03-02 (ML)	MAP02-28 (BL)
Locality[2]	AN	AN	AN	AN	Mon	AS	AS	AS	L-s-M	L-s-M
SiO_2	48.56	49.19	54.36	57.60	46.72	41.64	42.77	1.21	3.17	0.92
Al_2O_3	22.92	23.54	22.08	21.66	26.67	31.41	31.67	0.46	0.45	0.20
CaO	3.31	1.21	0.41	0.55	3.06	1.11	0.70	53.21	51.31	55.67
Cr_2O_3	0.010	0.00	<0.001	<0.001	0.018	0.003	0.003	<0.001	<0.001	0.001
Fe_2O_3	4.97	5.58	2.19	1.56	4.13	3.13	4.02	0.07	0.14	0.08
K_2O	1.92	0.31	0.16	0.13	3.70	1.38	1.78	0.05	0.09	0.04
MgO	6.44	9.02	8.63	8.63	2.13	2.94	2.79	0.70	0.57	0.47
MnO	0.073	0.10	0.023	0.018	0.060	0.008	0.020	0.009	0.009	0.003
Na_2O	0.18	0.10	0.03	0.01	0.17	0.22	0.51	0.03	0.02	0.02
P_2O_5	0.27	0.15	0.16	0.14	0.84	0.35	0.31	0.02	0.01	<0.01
TiO_2	0.48	0.33	0.33	0.32	0.68	0.77	0.84	0.01	0.02	0.01
LOI[3]	12.41	12.29	9.76	9.63	12.42	16.76	14.48	42.68	41.44	42.60
Ba	93.3	67.5	32.9	33.9	273.4	162.9	153.2	6.2	10.4	7.8
Ce	37.8	100.5	66.3	46.5	74.2	25.7	18.9	3.3	2.2	2.3
Dy	3.6	3.8	3.0	2.8	4.2	1.1	0.7	0.3	0.2	0.3
Er	2.6	1.9	1.5	1.4	2.1	0.7	0.5	0.1	0.1	0.2
Eu	0.6	0.6	0.5	0.4	0.7	0.2	0.2	<0.1	<0.1	<0.1
Ga	17.1	15.7	15.6	13.5	19.9	24.1	18.2	<0.5	0.6	<0.5
Gd	2.9	4.5	3.5	3.0	6.9	1.3	0.7	0.2	0.2	0.1
Hf	10	11	5	6	13	11	10	<1	<1	<1
Ho	0.8	0.7	0.6	0.5	0.7	0.2	0.2	<0.1	<0.1	<0.1
La	16.4	30.7	26.7	18.4	25.3	11.3	8.4	1.7	1.0	1.1
Lu	0.5	0.3	0.2	0.2	0.2	0.1	<0.1	<0.1	<0.1	<0.1
Nb	21.0	27.9	18.3	19.5	22.4	10.1	11.7	1.2	0.6	<0.5
Nd	13.7	31.1	22.6	17.8	44.4	9.2	6.6	1.6	0.9	1.0
Pr	3.8	9.6	6.7	5.0	10.1	2.5	1.9	0.4	0.3	0.3
Rb	50.8	10.8	3.5	2.1	105.8	36.2	45.9	1.6	4.4	1.5
Sc	14	11	9	9	10	5	8	<1	<1	<1
Sm	3.3	5.9	4.3	3.7	10.5	1.6	1.1	0.3	0.2	0.2
Sn	3	2	1	1	5	2	1	<1	<1	<1
Sr	47.9	14.9	15.7	6.9	176.6	128.5	594.0	572.4	314.3	413.6
Ta	2.8	3.1	1.8	2.3	3.3	2.0	2.1	1.1	0.2	0.1
Tb	0.6	0.7	0.5	0.5	0.9	0.2	0.1	<0.1	<0.1	<0.1
Th	29.4	39.1	26.1	27.1	84.9	58.9	55.6	0.3	0.2	0.1
Tm	0.4	0.3	0.2	0.2	0.3	0.1	<0.1	<0.1	<0.1	<0.1
U	28.0	14.5	8.2	6.4	13.8	9.4	16.8	7.3	1.4	1.7
V	126.6	57.5	18.0	16.8	77.9	83.0	81.2	17.2	17.0	22.3
W	1.4	11.1	1.5	1.0	4.0	9.1	1.7	1.4	5.9	1.0
Y	26.9	17.2	13.0	12.1	21.7	5.9	3.8	2.2	1.3	2.3
Yb	2.8	2.0	1.3	1.3	1.6	0.6	0.6	0.1	0.1	0.2
Zr	333	356	143	159	427	338	283	9	4	4
Eu/Eu*[4]	0.56	0.38	0.41	0.38	0.24	0.48	0.61	Eu <LoD	Eu <LoD	Eu <LoD
ΣREE	89.7	192.6	137.9	101.5	182.0	54.9	39.9	8.2	5.6	5.9

1. Samples comminuted using a TEMA tungsten carbide ring-and-puck mill are denoted by a number (#) sign; all other samples were comminuted in a Retsch agate ball mill. Data for samples marked with a plus sign are averages of two replicate analyses. BL = bioclastic limestone; ML = micritic limestone.
2. Sampling localities were as follows: AN = Anhée Nord (50.3180°N, 4.8758°E); AW = Awirs West Quarry (50.5905°N, 5.4089°E); AS = Anhée Sud (50.2940°N, 4.8936°E); Eng = Engihoul Quarry (50.5764°N, 5.4241°E); L-s-M =Lives-sur-Meuse (50.4692°N, 4.9291°E); Mal = Malonne (50.4339°N, 4.7952°E); Mon = Monceau (50.3984°N, 4.3751°E); Roy = Royseux (50.4690°N, 5.2679°E); Sos = Sosoye (50.3001°N, 4.7771°E; all co-ordinates relative to the WGS84 datum).
3. Loss-on-ignition determined at 1000°C.
4. Europium anomaly calculated using data normalised to CI-chondrite values (McDonough & Sun, 1995). LoD = limit of detection.

4.3. X-ray diffraction analysis

Samples were dried overnight at 80 °C and then powdered by hand using an agate mortar and pestle. Whole-rock powders were loaded as front-filled cavity mounts and run using a Philips PW1720 X-ray generator coupled to a Philips PW1050/25 diffractometer, housed in the Department of Geology, Trinity College Dublin. Analyses were obtained using Ni-filtered Cu kα radiation, a step size of 0.02 °2θ / s and operating conditions of 40 kV and 20 mA. Sample data were interpreted using the 'Traces' software program (from Hiltonbrooks Limited; http://www.xrays.u-net.com/Software.htm), which is equipped with the ICDD powder diffraction database, and also using the 2θ tables for common minerals of Chao (1969).

5. Results

Several previous studies have demonstrated that the major-element geochemistry of a bentonite is often significantly modified from that of the original ash during diagenesis (e.g. Christidis, 1998; Spears et al., 1999). Diagenetic modification of the Viséan NDB bentonites is suggested by the high Al concentrations (20 – 30% Al_2O_3) in many of the samples, which exceed what could reasonably be expected to occur in unaltered volcanic rocks, and probably originates from residual enrichment. Further geochemical complexity arises from the heterogeneous presence of carbonate within the bentonite horizons, which increases CaO and Sr concentrations whilst effectively diluting other elements. The combination of diagenetic modifications and heterogeneous limestone additions limit the usefulness of absolute concentrations. Instead, elemental ratios are used preferentially to inform on the magmatic parentage of these bentonites. Absolute concentrations are used only to highlight broad geochemical trends; i.e., bentonite samples exhibit a strong enrichment in the large-ion lithophile elements, decreasing enrichment in the high field strength elements and negative Nb anomalies (Fig. 3). Compared to the enclosing limestones, the bentonite samples typically show 3 to 100 times greater enrichment in all elements apart from Ca, Mn, Sr and U (Fig. 3; Ca and Mn not shown).

Samples taken from the base and top of bentonites L4, L6 and W8 yielded very similar elemental concentrations (Fig. 4), suggesting that there are no major vertical chemical variations in at least these three bentonites. There is a slight enrichment of light rare earth elements (LREE), P_2O_5, U and Th in the upper sample from bentonite L4 (Fig. 4), which may indicate a slightly greater concentration of apatite in this sample. Whilst most of the laterally equivalent bentonite samples show similar geochemistry and mineralogy within the same bentonite horizon, bentonites L3 to L6 from Awirs West and Engihoul quarries exhibit considerable mineralogical variation: the samples from Awirs West quarry contain probable mixed-layer clays and kaolinite, whereas the equivalent horizons at Engihoul quarry contain significant calcite, quartz and pyrite, plus small amounts of clay minerals (probable mixed-layer clays; Fig. 5). Despite these mineralogical differences, samples of bentonites L3 and L4 from Awirs and Engihoul quarries show similarities in geochemistry (e.g. TiO_2/Al_2O_3, ΣREE; Fig. 6), whereas samples of bentonite L6 show no such similarities (Fig. 6).

Excluding the sample of bentonite L6 from Engihoul quarry, some stratigraphic trends become apparent: Cr_2O_3/Al_2O_3 and TiO_2/Al_2O_3 ratios are strongly correlated throughout and show a systematic decrease between bentonites M and L3 (Fig. 6). P_2O_5/Al_2O_3 (not shown in Fig. 6) is exceptionally high in bentonites L2 and W9; with respect to bentonite L2, this correlates with the occurrence of abundant apatite grains in the heavy mineral fraction and apatite inclusions in zircon.

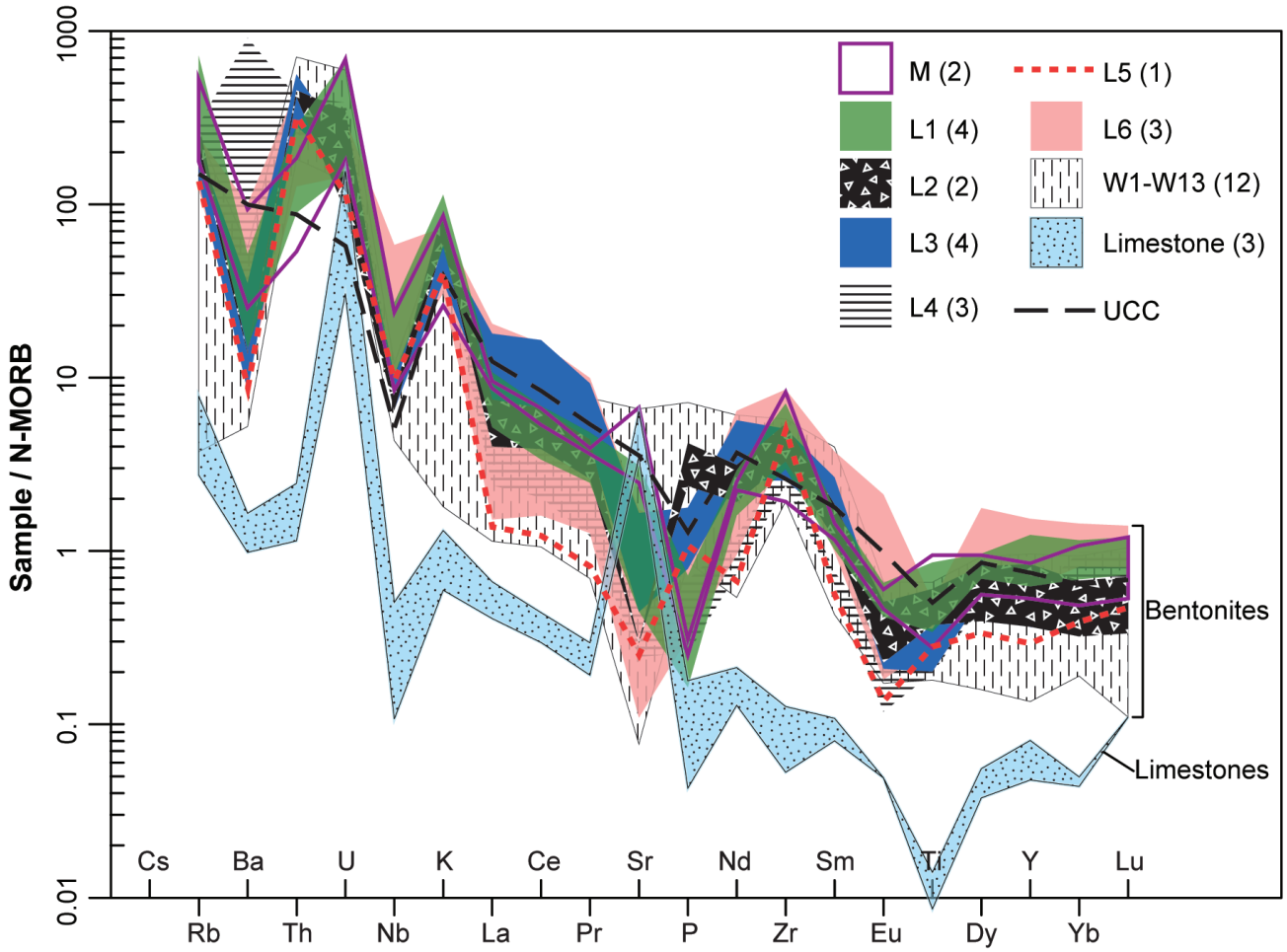

Figure 3. N-MORB normalised multi-element diagram. Sample data are drawn normalised to the N-MORB values of Sun & McDonough (1989). UCC = upper continental crust (after Rudnick & Gao, 2003). Numbers in brackets are the number of samples included in each field (includes samples from the base and top of bentonites L4, L6 and W8).

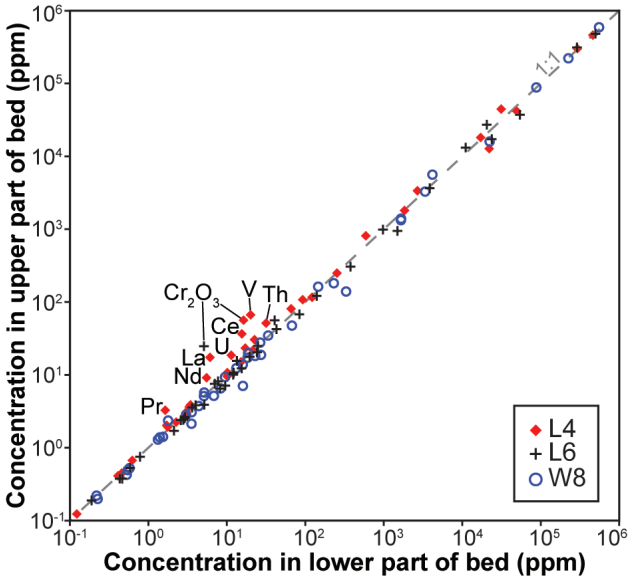

Figure 4. Scatter plot of element concentrations in samples from the base and top of bentonites L4, L6 and W8.

There is also a very prominent drop in K_2O/Al_2O_3 and increase in MgO/Al_2O_3 between bentonites W6 and W8 (Fig. 6). These bentonites contain measurable amounts of chlorite and have smaller concentrations (W6) or lack (W7, W8) illite-smectite mixed-layer clays (Fig. 5). The type(s) of chlorite cannot be determined from the whole-rock powder XRD data, but Al-Mg-rich chlorites including sudoite and clinochore have been reported from some of the 'W' bentonites at Anhée Nord (Anceau, 1992, 1996). The transitional nature of the change in K_2O/Al_2O_3, MgO/Al_2O_3 and clay mineralogy between bentonites W6 and W8 may record a short-term change in ash composition. Conversely, fluctuations in depositional environment linked to ocean connectivity have been argued to control the clay mineralogy of Namurian (Serpukhovian) bentonites within the Pennine Basin (Spears et al., 1999; Spears, 2006). Whilst such variations in depositional environment were not detected in the field for the limestone succession between bentonites W6 to W8, such environmental changes cannot be entirely excluded.

Most of the bentonites show a strong enrichment in LREE (Fig. 7), which dominates the ΣREE budget, and accounts for the strong correlation between La_N/Yb_N values and ΣREE ppm throughout the stratigraphic section (Fig. 6). In detail, however, there is some variation in La_N/Yb_N values between bentonite beds. The highest La_N/Yb_N values were obtained from bentonites L3 and W7 – W13 (La_N/Yb_N >9), and the lowest values from bentonites L4 – L6 (Fig. 6; La_N/Yb_N <4). All samples have strong negative Eu/Eu* anomalies (calculated as $Eu_N/\sqrt{Sm_N \times Gd_N}$, where N denotes concentrations normalised to CI-chondrite values) except for bentonites L4 and L6 from Engihoul quarry which have much smaller negative Eu/Eu* anomalies (0.62 and 0.73 cf. less than 0.53 for all other bentonites; Fig. 6). There is a strong inverse correlation between Eu/Eu* values and Zr/TiO_2 ratios upwards through the section, although the trend weakens between bentonite W3 and W7 (Fig. 6). Furthermore, there is evidence of a progressive decrease in Eu/Eu* value between bentonites M and L3 (Fig. 6), which is concomitant with an increase in Zr/TiO_2 ratios (Fig. 6). Studies by Wray (1995) and Wray & Wood (1998) have shown that normalising REE data to detrital shale values can be used to differentiate between detrital and volcanogenic clay-rich beds. When presented as shale-normalised REE profiles, detrital clay-rich beds are characteristically subhorizontal whilst bentonites typically exhibit negative Eu/Eu* anomalies, a depletion of LREE, and a depletion or enrichment of heavy REE (HREE; Wray & Wood, 1998). Most of the NDB bentonites show similar shale-normalised REE trends that are characterised by a

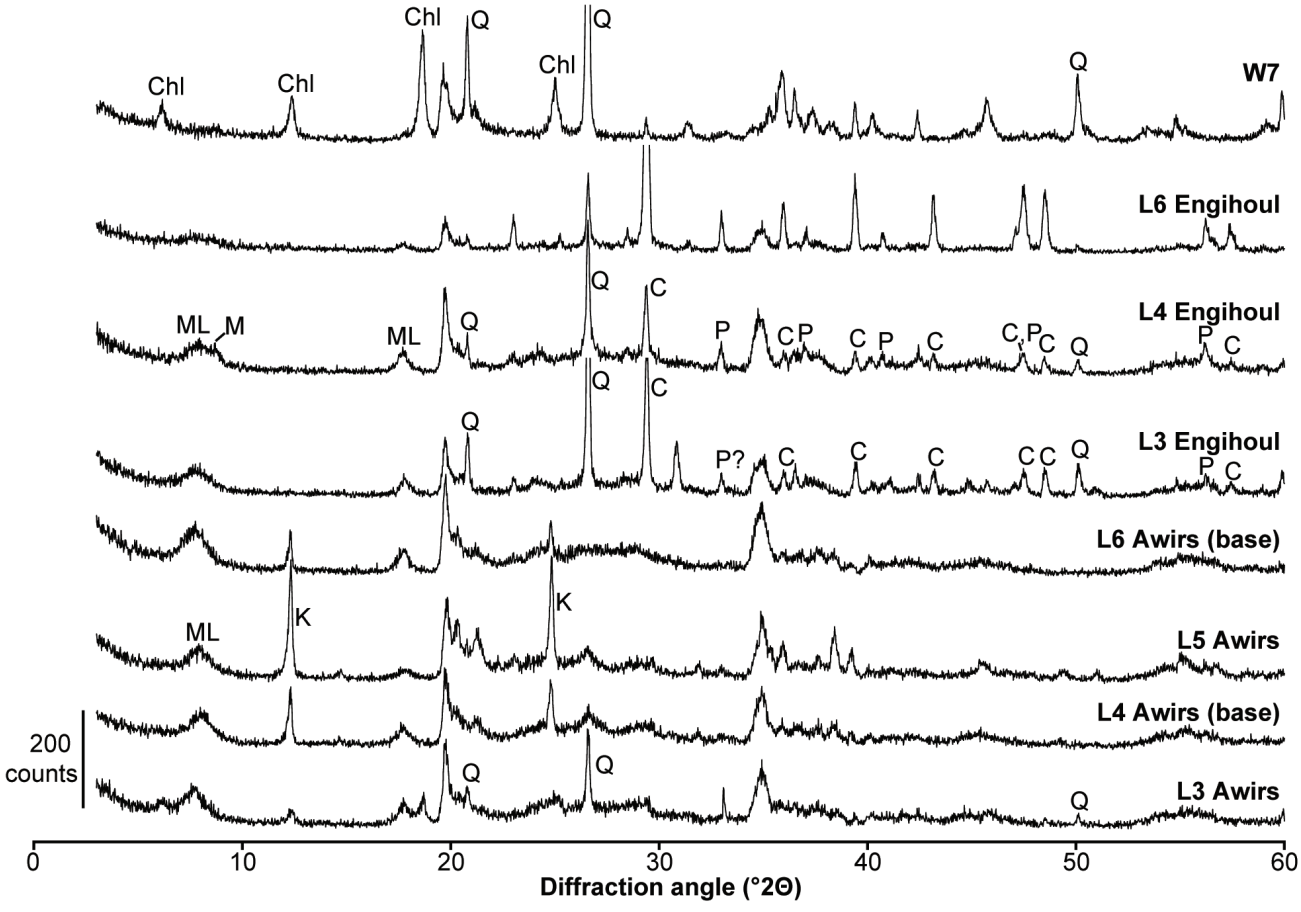

Figure 5. Whole-rock powder X-ray diffraction traces. C = calcite; Chl = chlorite; M = illite / mica; ML = probable mixed-layer clay; K = kaolinite; P = pyrite; Q = quartz.

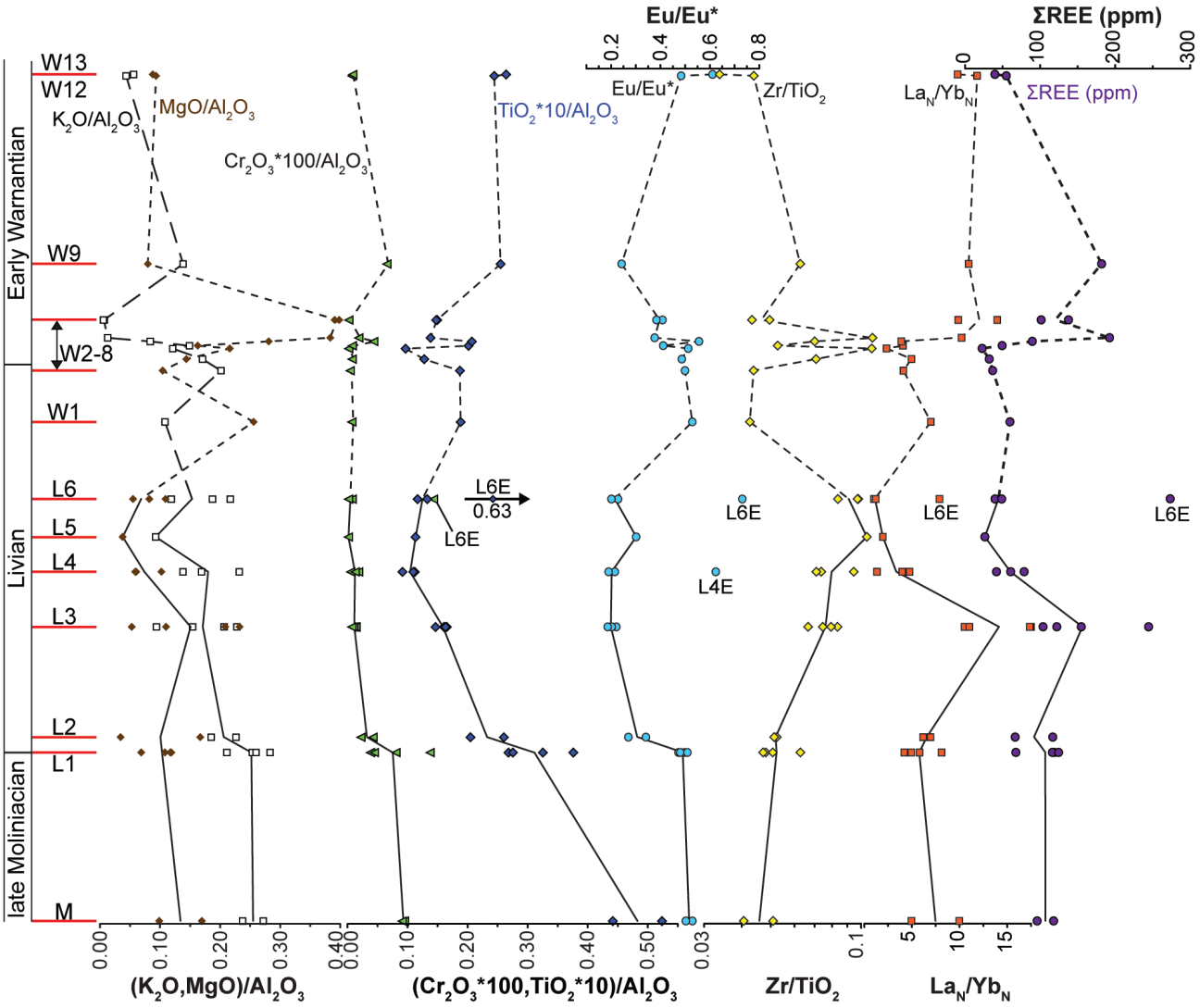

Figure 6. Stratigraphic column showing vertical geochemical variations between the bentonite horizons. Solid lines drawn between bentonites M and L6 are cubic splines calculated from laterally equivalent samples. Dashed lines connect data from bentonite horizons with only one sample. All axes are linear except for Zr/TiO_2 which is logarithmic. L4E and L6E are bentonites L4 and L6 from Engihoul quarry. La_N and Yb_N denote La and Yb concentrations that are normalised to CI-chondrite values (after McDonough & Sun, 1995).

depletion in LREE, prominent negative Eu/Eu* anomalies and variable depletion in HREE (Fig. 7). The exceptions are the two bentonites collected from Engihoul quarry: L6 is characterised by a subhorizontal trend, whereas L4 lacks a shale-normalised Eu/Eu* anomaly (Fig. 7).

In felsic igneous rocks, whilst the major elements are hosted largely in the main rock-forming minerals, the trace element budget is commonly controlled by accessory minerals (Wark & Miller, 1993; Bea, 1996; Hoskin et al., 2000; Claiborne et al., 2010). These include apatite and zircon, which are both ubiquitous phenocrysts in the Viséan NDB bentonites. Zircon is a significant host of Ce, Hf, Th, U and HREE (Bea, 1996; Belousova et al., 2002a; Hoskin & Schaltegger, 2003). Belousova et al. (2002a) further identified zircon as a host for Nb and Ta. Zircons from different rock types show a wide range in trace element concentrations, although in general concentrations increase with magmatic fractionation and range from ppm to percent (Belousova et al., 2002a). Apatite occurs as inclusions in zircon and as discrete grains within the NDB bentonites. Apatite can host significant amounts of Y and REE (ppm to percent), and typically exhibits a greater enrichment in LREE compared to HREE, although REE fractionation has been observed to correlate negatively with magmatic fractionation (Belousova et al., 2002b). Like zircon, Y and HREE concentrations in apatite typically increase with magmatic fractionation (Belousova et al., 2002b). It is feasible, therefore, that many of the trace elements that are routinely used to classify altered volcanic rocks (Hf, Nb, Ta, Ti, Y, Zr and REE) reside mostly in the unaltered apatite and zircon phenocrysts within the NDB bentonites. Negative Eu/Eu* anomalies are common in both igneous apatite and zircon; moreover, the magnitude of negative Eu/Eu* anomaly has been observed to correlate positively with magmatic fractionation (Hoskin et al., 2000; Belousova et al., 2002a, 2002b; Claiborne et al., 2010). Negative Eu/Eu* anomalies in igneous apatite and zircon have largely been attributed to the partitioning of Eu into feldspar and the subsequent removal of feldspar from the melt during fractional crystallisation (e.g. Hoskin et al., 2000; Belousova et al., 2002a, 2002b; Hoskin & Schaltegger, 2003), although Eu is redox sensitive, and consequently reducing conditions in the melt can also generate negative Eu/Eu* anomalies (Hoskin & Schaltegger, 2003; Trail et al., 2012). Opaque accessory minerals are ubiquitous in the NDB bentonites (Thorez & Pirlet, 1979) and are probably the hosts for Cr and Ti. Anatase has been reported from some of the NBD bentonites (Anceau, 1993) and is another potential reservoir for Ti.

Classification and tectonic discrimination diagrams are widely used in geochemical studies of bentonites to infer original ash compositions and the tectonic settings of the source volcanoes where direct petrogenetic and geological constraints are not available. Their usage, however, is controversial. This is because many diagrams employ absolute elemental concentrations, which are difficult to apply to bentonites because diagenetic alteration may render elemental abundances dissimilar to those of the original unaltered

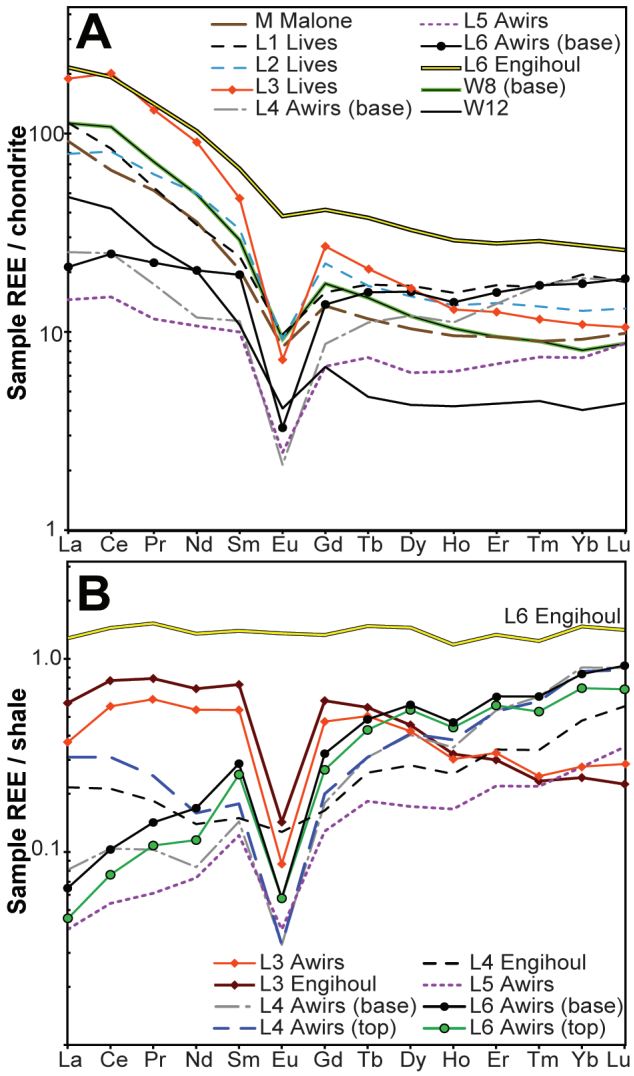

Figure 7. Rare earth element plots for several Viséan bentonite samples. Bentonite data are drawn normalised to: (A) CI-chondrite (after McDonough & Sun, 1995); and (B) Cody Shale (after Govindaraju, 1994).

volcanic ash (e.g. through residual enrichment or element mobility). Furthermore, several studies have raised concerns about the efficacy of a number of widely-used tectonic discrimination diagrams developed during the 1970s and 1980s (e.g. Wang & Glover, 1992; Snow, 2006; Li et al., 2015). This is because such diagrams were constructed using limited datasets that under-represent the extent of geochemical variation in igneous rocks from different tectonic settings. Thus, caution should be exercised when using classification and discrimination diagrams, particularly for ancient altered volcanic rocks whose source cannot be established from field evidence. When sample trace element data from the Belgian bentonites are plotted on the Nb/Y versus Zr/TiO_2 discrimination diagram of Winchester & Floyd (1977), the samples form a cluster within the trachyandesite and trachyte fields (Fig. 8A). Studies by Christidis (1998) and Hill et al. (2000) have demonstrated that yttrium can be lost during the alteration of volcanic rocks to bentonites, and therefore the inferred alkalinity of the studied bentonites should be considered a maximum estimate. Using the two tectonic discrimination diagrams of Gorton & Schandl (2000) and Schandl & Gorton (2002) that employ elemental ratios, all but five samples plot within the active continental margins field (Fig. 8B-C). Of the remaining five samples, the two samples from bentonite M and bentonite L1b from Sosoye plot in the within plate volcanic zones field, L6 from Engihoul quarry plots in the within plate basalts field and bentonite W12 plots in the oceanic arcs field (Fig. 8B).

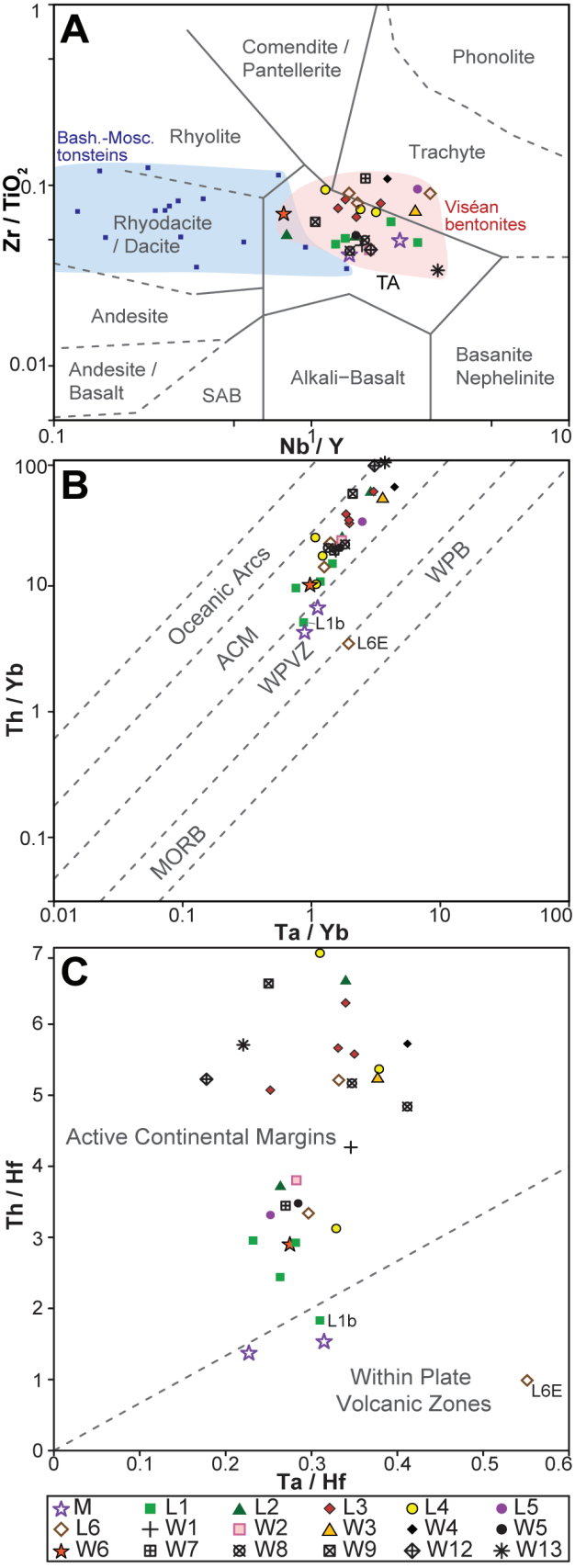

Figure 8. Bentonite geochemical data plotted on several geochemical classification and tectonic discrimination diagrams (drawn using GCDKit v.4; Janoušek et al., 2006). (A) Nb/Y versus Zr/TiO_2 classification diagram (after Winchester & Floyd, 1977). SAB = sub-alkaline basalt; TA = trachyandesite. (B-C) Hf-Ta-Th-Yb tectonic discrimination diagrams (after Gorton & Schandl, 2000; Schandl & Gorton, 2002). ACM = active continental margins, MORB = mid-ocean ridge basalts, WPB = within plate basalts, WPVZ = within plate volcanic zones. L6E is bentonite L6 from Engihoul quarry. Bashkirian-Moscovian tonstein data are redrawn from Spears & Lyons (1995) and Pointon (2012).

6. Discussion

6.1. Lateral variations within bentonites L4 and L6

The geochemistry and mineralogy of most of the bentonites analysed do not vary much laterally. The exceptions are bentonites L4 to L6 from Awirs West and Engihoul quarries. There appears to be an up-section divergence in geochemistry between bentonites L3, L4 and L6 from these two quarries as: samples of bentonite L3 from each quarry are geochemically similar; samples of bentonite L4 exhibit similar trace element geochemistry apart from Eu/Eu* anomalies (Figs 6 - 8); but samples of bentonite L6 show strong dissimilarities in trace element geochemistry (Figs 6 - 8). The reason(s) for these lateral variations are unclear. Miscorrelation is unlikely because of the uniformity of the stratigraphy: individual carbonate parasequences can be correlated reliably between these localities, which are <2 km apart (Fig. 1), using parasequence thickness and the varying proportions of micritic and bioclastic limestone within the parasequences. Recent weathering, likewise, cannot account for all of the mineralogical differences. The mineralogical and geochemical differences are instead interpreted as real lateral variations in composition between these bentonites. The abundance of quartz and calcite in bentonites L4 and L6 at Engihoul quarry, the flat shale-normalised REE profile of bentonite L6 (Fig. 7), and the absence of quartz and calcite from the same horizons at Awirs West quarry suggests that bentonites L4 and L6 from Engihoul quarry are contaminated by sedimentary detritus or have been affected by diagenetic fluids. Regardless of the cause, the data strongly suggest that the volcanogenic component has been diluted in bentonites L4 and L6 from Engihoul quarry, and to a greater extent in bentonite L6. This may explain why bentonite L6 from Engihoul quarry plots separately in Fig. 8B-C. As a consequence of this interpretation, data from bentonite L6 at Engihoul quarry is excluded from the following discussion about magmatic parentage.

6.2. Magmatic parentage and tectonic setting

Classification using the Nb/Y versus Zr/TiO_2 discrimination diagram (Fig. 8A) suggests that the studied bentonites were originally predominantly evolved, mildly alkaline to alkaline, trachyandesitic to trachytic ashes. As discussed above in section 5, the inferred alkalinity is a maximum estimate. Additional support for a mildly alkaline ash composition is obtained through comparison of geochemistry data from the NDB bentonites with equivalent data from Permian tonsteins (kaolinitic, diagenetically altered, volcanic ash layers) in the Songzao Coalfield, China (Dai et al., 2011; Table 2). Dai et al. (2011) characterised three types of tonstein (mafic, silicic, and alkali) that were differentiated using TiO_2/Al_2O_3 ratios and a suite of trace and rare earth elements. In brief, alkali tonsteins show significant enrichment in Nb, Ta, Zr, Hf, REE, and Ga, whilst silicic tonsteins have low REE concentrations but exhibit the greatest fractionation between LREE and HREE (Dai et al., 2011; Table 2). Using the same geochemical indices, NDB bentonites yield value ranges between and partially overlapping those of the silicic and alkali tonsteins (Table 2). This is interpreted to support an intermediate (mild) alkalinity for the NDB bentonites.

The evolved, felsic magmatic parentage inferred for the NDB bentonites from the Nb/Y versus Zr/TiO_2 discrimination diagram (Fig. 8A) is further supported by the ubiquity of euhedral zircon, as well as the occurrence of splintery quartz (Thorez & Pirlet, 1979; Delcambre, 1989), Li-rich chlorite pseudomorphs after Li-rich biotite (Anceau, 1996) and sizeable negative Eu/Eu* anomalies. The negative Eu/Eu* anomalies in the NDB bentonites are interpreted here as a primary magmatic, geochemical feature, as has been inferred in studies of other bentonites (e.g. Wray, 1995; Huff et al., 1996). This is supported by the strong correlation between negative Eu/Eu* anomaly magnitude and Zr/TiO_2 ratios (Fig. 6), which are sensitive to magmatic fractionation (Winchester & Floyd, 1977; Floyd & Winchester, 1978). It is unlikely that the anomalies are caused by processes during diagenesis and burial metamorphism (Eu is redox sensitive and can be mobilised under highly reducing conditions; Sverjensky, 1984; Wray, 1995) and more probable that they are a magmatic feature preserved, at least in part, in the unaltered apatite and zircon phenocrysts.

Using the tectonic discrimination diagrams of Gorton & Schandl (2000) and Schandl & Gorton (2002), the vast majority of samples plot within the active continental margins field (Fig. 8B-C). The bentonites also have negative Nb anomalies and are enriched in large ion lithophile elements and LREE compared to the HFSE (Fig. 3), which are features of magmatism in an active continental margin setting (Pearce, 1982; Pearce & Peate, 1995; Baier et al., 2008). These geochemical characteristics are, however, not unique to active continental margins and can occur in magmatic rocks from other tectonic settings; for example, magma generated in an anorogenic continental setting can gain arc-like geochemical characteristics through extensive crustal assimilation (Thompson et al., 1982; Pearce et al., 1984; Pearce, 2014). Alternatively, the melting of sub-continental lithospheric mantle (SCLM) with an inherited subduction signature could also generate these geochemical characteristics (e.g. Turner et al., 1996; Benito et al., 1999). Of the four samples that plot outside the active continental margins field in Fig. 8B, bentonite W12 plots within the oceanic arcs field, albeit very close to the boundary with the active continental margins field. This is likely a misclassification as the oceanic arcs field was defined based on a very limited dataset by Gorton & Schandl (2000) and bentonite W12 has very similar geochemical characteristics to the other NDB bentonites. Bentonite L1b plots inconsistently with the other three samples from bentonite L1 (Fig. 8B-C). This is the only sample from bentonite L1 to contain significant carbonate (25.3% CaO); the high proportion of carbonate in this

	NDB bentonites	Songzao Coalfield tonsteins		
		Alkali	Silicic	Mafic
TiO_2/Al_2O_3	0.009 – 0.052	0.037 – 0.079	<0.02	0.087 – 0.119
Ga/Al_2O_3	0.29 – 1.67	1.5 – 2.22	0.57 – 1.1	1.02 – 2.83
Zr/Al_2O_3	6.5 – 26.7	15.5 – 357	2.2 – 6.5	20.7 – 126.2
Hf/Al_2O_3	0.23 – 0.7	0.36 – 4.8	0.09 – 0.2	0.74 – 4.6
Nb/Al_2O_3	0.3 – 2.5	1.6 – 6.3	0.2 – 0.5	8.8 – 16.7
Ta/Al_2O_3	0.06 – 0.16	0.11 – 0.39	0.06 – 0.1	0.3 – 1.4
ΣREE (ppm)	<247	44 – 1503	145 – 388	190 – 5860
$(La/Yb)_N$ [1]	1.0 – 17.6	3.2 – 14.9	18.1 – 46.4	2.2 – 21
Number [2]	30	13	5	17

Table 2. Comparison of whole-rock geochemistry data from Viséan NDB bentonites to Permian mafic, silicic and alkali tonsteins of the Songzao Coalfield, China (Dai et al., 2011). Data are expressed as minimum and maximum ranges. Data from bentonite L6 at Engihoul quarry were excluded from the comparison.

1. Calculated using data normalised to CI-chondrite values (McDonough & Sun, 1995).
2. Number of analyses used to calculate the data ranges.

bentonite probably arises because of brecciation towards the base of the bentonite and because of difficulties obtaining a pure sample from such a thin bentonite (maximum thickness of *c*. 2 cm). Elsewhere within the NDB, local pedogenesis of bentonite L1 has been reported (e.g. Poty & Hance, 2006a). It is possible that the brecciation of L1b at Sosoye is related to pedogenesis, although further study is required to confirm this. The distinct geochemistry of bentonite L1b could be interpreted to indicate that bentonite L1 comprises several ashes from multiple distinct volcanic sources, although it is more likely that the high carbonate concentration in bentonite L1b has compromised the trace element geochemistry of this sample. The two samples from bentonite M, only one of which contains substantial limestone (M from Malonne), plot together in the within plate volcanic zones field in Fig. 8B-C. Euhedral zircons in bentonite M are dominated by monoprismatic zircons ($N_{4,5}$ and K subtypes; Delcambre, 1989, 1996), which are indicative of an anorogenic, alkaline source according to the zircon typology classification diagrams of Pupin (1980). This is consistent with the within plate volcanic zones classification in Fig. 8B-C. In contrast, euhedral zircon populations in bentonites L1 – L3 and W1 – W12 have shapes that are indicative of an orogenic, calc-alkaline series, rhyolitic magmatic composition (Delcambre, 1989, 1996) according to the classification diagrams of Pupin (1980). Moreover, bentonite M contains abundant rounded zircons as well as tourmaline, rutile and sparse garnet which indicate detrital contamination. It is not clear whether these grains represent post-eruption detrital contamination or pre-eruption assimilation of country rock (Delcambre, 1996). Regardless of their source, however, the possibility that non-volcanogenic additions have modified the whole-rock geochemistry of bentonite M cannot be excluded. Due to uncertainties regarding the geochemistry and age of bentonite M, the possible locations of the volcanoes which sourced this bentonite are not discussed.

6.3. Possible locations of the source volcanoes

The lack of coeval *in situ* extrusive igneous rocks within the NDB implies an extra-basinal volcanic source for the Viséan bentonites. Lateral bentonite thickness variations have been used to infer paleowind directions in other studies of bentonites (e.g. Elder, 1988; Kiipli et al., 2008), although these are likely to be of limited use in this instance because of post-depositional Variscan deformation, particularly within the Ardenne Allochthon (Fig. 1).

By comparing maximum grain sizes of phenocrysts in Permian bentonites from the Saar–Nahe Basin, Germany, with equivalent published data from recent volcanic eruptions, Königer et al. (2002) estimated that maximum ash transport distances were probably less than 300 km. Maximum transport distances of fine-grained volcanic particles are difficult to predict because they are influenced by several factors including the height of the eruption column, atmospheric conditions such as wind strength and direction, as well as grain size, density, shape and surface roughness (e.g. Walker, 1971; Wilson & Walker, 1987). In general, however, crystal size decreases and aeolian fractionation occurs downwind of the vent; thus, dense minerals such as euhedral zircons with relatively smooth surfaces and small surface areas should experience relatively short transport distances (Königer et al., 2002). The eruption column heights of the volcanoes that sourced the NDB bentonites are unknown. Likewise, wind patterns within western Europe during Viséan times are poorly constrained and their prediction is limited by uncertainties in regional paleogeographic reconstructions. Nevertheless, using the same approach as Königer et al. (2002) and comparing maximum zircon grain sizes to published data from other distal ash fall tuffs suggests maximum transport distance on the order of 180 to 350 km for maximum zircon grain sizes of between 150 (bentonite W8) and 400 μm (bentonite L2 at Lives-sur-Meuse). This estimate suggests a proximal volcanic source and excludes a source from within the Uralian orogenic belt (>3000 km away; present day distance). Furthermore, the short transport distances envisaged would have limited the amount of aeolian fractionation and thus it is conceivable that the trace element geochemistry of these bentonites still approximates that of the ashes at the eruption site(s).

Viséan volcanism is well documented within the UK and Ireland from areas including the Midland Valley, Scotland (Monaghan & Parrish, 2006), Derbyshire (Timmerman, 2004), and the Limerick Basin, Ireland (Strogen, 1988; Somerville et al., 1992). In these areas, however, volcanism is of predominantly mafic composition and intra-plate affinity (Stephenson et al., 2003; Timmerman, 2004), which is incompatible with the trachyandesitic to trachytic compositions inferred for the NDB bentonites.

Within the exposed remnants of the Variscan orogenic belt there are plutonic and volcanic rocks of similar age and geochemistry to the NDB bentonites. There are several known Viséan intermediate to felsic (SiO_2 55 – 70%), high-Mg-K granitoid rocks (diorite, monzonite, syenite and granite; Schaltegger, 1997) that occur in a discontinuous belt parallel to the axis of the Variscan orogen (Fig. 9A; Finger et al., 1997; Schaltegger, 1997; Kotková et al., 2010; von Raumer et al., 2014). Many of these granitoids, including those of southern Vosges and the Black Forest, were intruded into Viséan volcano-sedimentary sequences at shallow depths (Schaltegger et al., 1996; Schaltegger, 1997, 2000). The geodynamic setting of these granitoids is debated, although it is generally agreed that they were derived from an enriched SCLM source, variably modified by crustal contamination (Schaltegger & Corfu, 1992; Finger et al., 1997; Schaltegger, 1997; von Raumer et al., 2014). SCLM enrichment under the Variscan orogen has been suggested to have arisen from protracted subduction (von Raumer et al., 2014). The geochemistry of the NDB bentonites is compatible with such a magmatic source; the subduction signature (negative Nb anomalies, enrichment of large ion lithophile elements and LREE over high field strength elements) could have originated from an enriched mantle source, or alternatively been acquired through crustal assimilation. Furthermore, available U–Pb dates from these intrusions cluster between 345 Ma and 330 Ma (Fig. 9B; summarised in Kotkova et al., 2010 and Tabaud et al., 2014), and are thus indistinguishable from the U–Pb zircon CA-ID-TIMS dates obtained from the NDB bentonites (340 – 332 Ma; Fig. 2). It is, therefore, possible that the NDB bentonites are an extrusive expression of these intrusions. Viséan volcanic and volcaniclastic rocks are preserved in sedimentary basins within the French Massif Central, southern Vosges and Black Forest regions (Fig. 9A). Direct evidence of Viséan volcanism in the Bohemian Massif is sparse; however, volcanic clasts within Viséan conglomerates of the Drahany Culm Basin suggest Viséan volcanism was not restricted to the western parts of the Variscan orogenic belt (Zachovalová & Leichmann, 2003).

Within the southern Vosges Basin, volcanic strata are observed at four levels in the middle to late Viséan sedimentary succession (Fig. 9C). The oldest volcanic strata are shallow submarine, sub-alkaline, andesitic lavas and pyroclastics (Coulon et al., 1975; Lefevre et al., 1994; Lakhrissi, 1996) and predate bentonite L1 on the basis of available U–Pb ID-TIMS dates from volcanic horizons above and below this interval (*c*. 345 – 342 Ma; Fig. 9C, Schaltegger et al., 1996). The second oldest package of volcanic strata comprises subaqueous trachyandesitic to trachytic volcanic rocks overlain by subaerial lavas and ignimbrites of quartz latitic and rhyolitic composition that were principally derived locally from the Molkenrain stratovolcano (Coulon et al., 1979). This volcanic package is dated to between *c*. 342 and 340 ± 2 Ma on the basis of U–Pb multi-grain zircon ID-TIMS analyses from rhyolites close to the base and top of the package (Schaltegger et al., 1996), although there is complexity within the U–Pb dataset: a second rhyolite sample from the top of the volcanic package yielded a younger U–Pb date of 336 $^{+3}/_{-5}$ Ma (Schaltegger et al., 1996). Thus, it is unclear whether this volcanic interval is coeval or older than the Viséan NDB bentonites. Modern single-grain U–Pb zircon CA-ID-TIMS analyses from the southern Vosges volcanic rocks are needed to test further the synchronicity between this volcanic

episode and the Viséan NDB bentonites. The two youngest volcanic packages comprise trachyandesitic and trachytic lavas and breccias, and rhyodacitic ignimbrites respectively (Fig. 9C; Coulon et al., 1975; Lakhrissi, 1996). These volcanic packages have been assigned a late Viséan age (e.g. Coulon et al., 1975; Schneider et al., 1989), although there are no direct absolute age constraints. Lithological similarities have been drawn between the thick (>400 m) rhyodacitic ignimbrites and the Tuff Anthracifères of the Massif Central, which are also subaerial, sub-alkaline dacitic to rhyolitic ignimbrites

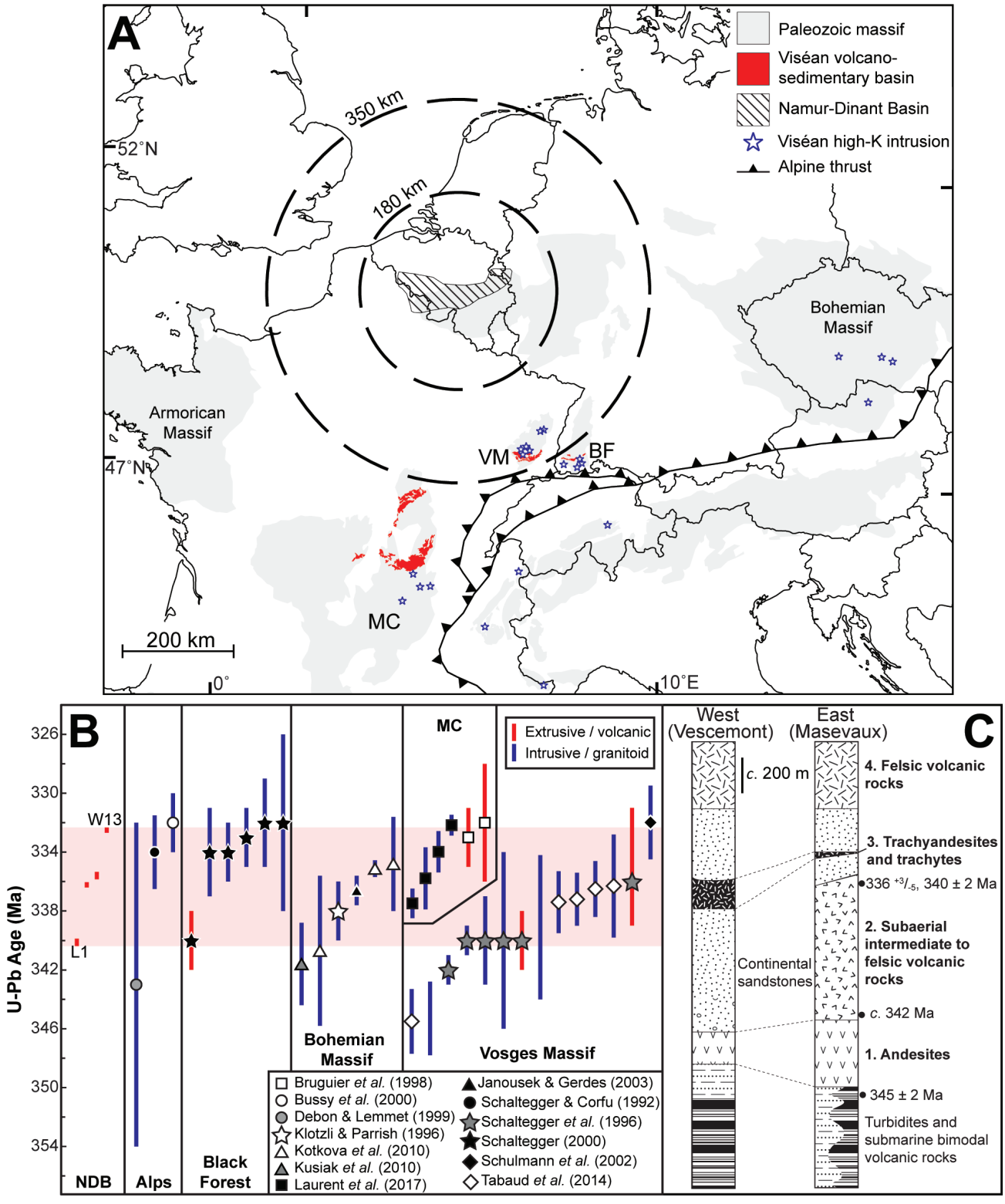

Figure 9. (A) Map of Europe showing the location of the Namur-Dinant Basin and estimated maximum ash transport distances based on maximum zircon grain size. Viséan intrusive rocks dated using the U–Pb method are mapped from: Alpine massifs = Schaltegger & Corfu (1992), Bussy et al. (2000); Debon & Lemmet (1999), Rubatto et al. (2001); Black Forest = Schaltegger (2000); Bohemian Massif = Janoušek & Gerdes (2003), Klötzli & Parrish (1996), Kusiak et al. (2010), Kotková et al. (2010); Massif Central = Laurent et al. (2017); Vosges Massif = Schaltegger et al. (1996), Tabaud et al. (2014), Schulmann et al. (2002). Viséan volcano-sedimentary basins are redrawn using 1:1,000,000 national and 1:1,500,000 European geological maps accessed through the OneGeology initiative website (www.OneGeology.org). BF = Black Forest; MC = Massif Central; VM = Vosges Mountains. (B) U–Pb ages from Variscan Viséan intrusive and volcanic rocks. All dates are drawn at the 2σ / 95% confidence level. NDB = Namur-Dinant Basin bentonites. The shaded horizontal band represents the time interval between bentonites L1 and W13. U–Pb bentonite dates are from Pointon (2012) and Pointon et al. (2014). (C). Schematic stratigraphic column of the southern Vosges Basin redrawn and simplified from Coulon et al. (1975). U–Pb dates are from Schaltegger et al. (1996); stratigraphic positions of the dated samples are approximate.

(Delfour, 1989; Schneider et al., 1989; Lardeaux et al., 2014). The latter have been dated in two basins of the Massif Central using the U–Pb zircon ID-TIMS method and have yielded U–Pb dates of *c*. 332 – 333 Ma (Bruguier et al., 1998; Fig. 9B).

Within the Badenweiler-Lenzkirch zone, southern Black Forest, there are sub-alkaline high-K to shoshonitic dacitic and rhyolitic tuffs, lapilli tuffs, pyroclastic breccias and lava flows (Güldenpfennig & Loeschke, 1991; Schaltegger, 2000) which have been dated using the U–Pb zircon ID-TIMS method (*c*. 340 – 332 Ma; Schaltegger, 2000) and are coeval with the NDB bentonites. In the Massif Central, rare trachytes and latites have been reported from late Viséan strata beneath the Tuff Anthracifères (Schneider et al., 1989), although there are no absolute age constraints from these strata. The majority of middle to late Viséan volcanic rocks in both the Massif Central and southern Black Forest have a sub-alkaline geochemistry (Delfour, 1989; Güldenpfennig & Loeschke, 1991; Lardeaux et al., 2014). Provided that the alkalinity estimates for the NDB bentonites based on Nb/Y ratios are representative of the original ashes, the southern Vosges Massif is a more likely source area than the Black Forest or Massif Central. This is because of the greater incidence of trachyandesite and trachyte volcanism reported from the southern Vosges Massif.

6.4. Comparison to late Baskhirian to Moscovian tonsteins of Western Europe

Numerous late Baskhirian to Moscovian (Westphalian) tonsteins are known from Late Carboniferous coaliferous basins across western Europe, including Britain, France, Belgium and Germany (e.g. Bouroz, 1967; Fiebig, 1967; Spears & Kanaris-Sotiriou, 1979; Delcambre, 1987, 1996). Based on trace element geochemistry, felsic Westphalian tonsteins of the Pennine, Campine and Ruhr basins were originally subalkaline, intermediate to felsic ashes (Fig. 8A); i.e, they are similarly evolved but less alkaline than the Viséan NDB bentonites. Some of the Westphalian tonsteins have been isotopically dated using the U–Pb zircon CA-ID-TIMS method, and have yielded *c*. 313 – 318 Ma ages (Pointon et al., 2012; Waters & Condon, 2012). These are significantly younger than the Viséan NDB bentonites; however, previous workers have hypothesised that these tonsteins were also derived from within the Variscan Orogenic Belt. Based on bed thickness and grain size variations, Bouroz (1967) suggested that Westphalian tonsteins within the Nord-Pas de Calais and Saar-Lorraine basins were derived from the southeast, possibly from the Vosges Massif or Black Forest. Subsequently, Spears & Kanaris-Sotiriou (1979) correlated several Westphalian tonsteins in the Pennine Basin, United Kingdom, with tonsteins in the Nord-Pas de Calais and Ruhr basins, and hypothesised that they shared a common volcanic source. Spears & O'Brien (1994) elaborated on this by suggesting that the British tonsteins were sourced from volcanoes related to I-type granitic plutons within the Variscan orogenic belt. These I-type plutons form a belt-like configuration over 1000 km long within the Alpine-Carpathian Chain (Spears & O'Brien, 1994; Finger et al., 1997). It is noteworthy that age and inferred ash chemistry of the Viséan NDB bentonites and Westphalian tonsteins closely correspond with known magmatic pulses within the Variscan orogenic belt (cf. Finger et al., 1997; Schaltegger, 1997). This strengthens the argument that these bentonites and tonsteins were sourced from the Variscan orogenic belt, and that selected trace elements within these layers provide a reliable record of original (unaltered) volcanic ash composition.

7. Conclusions

Whole-rock geochemical analysis of several Carboniferous (Viséan; Moliniacian to Warnantian) bentonites from the Namur-Dinant Basin, southern Belgium, was undertaken to provide insight into the original magmatic composition of these diagenetically altered volcanic ash layers. Their trace element geochemistry suggests most of the bentonites were originally trachyandesitic to trachytic ashes. A Variscan source for these bentonites is most likely based on proximity, and comparisons with zircon U–Pb isotopic age and whole-rock geochemistry data from literature sources. A source from within the Uralides or Britain and Ireland can be excluded on distance and geochemical grounds respectively. Within the Variscan orogenic belt, the southern Vosges region is the closest potential source area and contains volcanic rocks of comparable age and geochemistry. Provided that the alkaline parentage inferred from Nb/Y ratios for the NDB bentonites is accurate, then the southern Vosges region, where there is evidence of trachyandesite and trachyte volcanism, is a more likely source area than the Black Forest or Massif Central. There are a significant number of high Mg-K intrusions of compatible age in the Bohemian Massif but records of contemporaneous volcanism are sparse, making it difficult to evaluate whether this was a potential source area for the NDB bentonites. Significant ash contributions from the more distal Variscan massifs, such as those within the Alps, cannot be excluded, but are considered less likely because of the greater intervening distances between these massifs and the NDB during Viséan times.

8. Acknowledgements

Carmeuse S.A. is thanked for allowing us to sample bentonites exposed within the Awirs West and Engihoul quarries. Robbie Goodhue (Trinity College Dublin) is thanked for assistance with the XRD analyses. Maria Ovtcharova (University of Geneva) is thanked for help with the U–Pb zircon CA-ID-TIMS dating of bentonite L1. This research is based upon work supported by a Science Foundation Ireland (SFI) Research Frontiers Programme grant (ID: 07-RFP-GEOF207). D.A. Spears, editor A. Anceau and an anonymous reviewer are gratefully acknowledged for constructive, thought-provoking comments and suggestions that have improved this manuscript.

9. References

Anceau, A., 1992. Sudoite in some Visean (Lower Carboniferous) K-Bentonites from Belgium. Clay Minerals, 27, 283–292.

Anceau, A., 1993. Caractérisation des minéraux argileux des bentonites potassiques du Carbonifère inférieur de la Belgique et des régions limitrophes. Unpublished PhD thesis. Université de Liège, Belgium, 165 p.

Anceau, A., 1996. Sudoite, Al-rich Li-Mg-bearing chlorite, clinochlore and kaolinite as alteration products of biotite in Visean K-bentonites from Belgium. European Journal of Mineralogy, 8, 493–506.

Baier, J., Audétat, A. & Keppler, H., 2008. The origin of the negative niobium tantalum anomaly in subduction zone magmas. Earth and Planetary Science Letters, 267, 290–300.

Barham, M., Murray, J., Sevastopulo, G.D. & Williams, D.M., 2015. Conodonts of the genus *Lochriea* in Ireland and the recognition of the Viséan-Serpukhovian (Carboniferous) boundary. Lethaia, 48, 151–171.

Bea, F., 1996. Residence of REE, Y, Th and U in granites and crustal protoliths; Implications for the chemistry of crustal melts. Journal of Petrology, 37, 521–552.

Belousova, E.A., Griffin, W.L., O'Reilly, S.Y. & Fisher, N.I., 2002a. Igneous zircon: trace element composition as an indicator of source rock type. Contributions to Mineralogy and Petrology, 143, 602–622.

Belousova, E.A., Griffin, W.L., O'Reilly, S.Y. & Fisher, N.I., 2002b. Apatite as an indicator mineral for mineral exploration: trace-element compositions and their relationship to host rock type. Journal of Geochemical Exploration, 76, 45–69.

Benito, R., López-Ruiz, J., Cebriá, J.M., Hertogen, J., Doblas, M., Oyarzun, R. & Demaiffe, D., 1999. Sr and O isotope constraints on source and crustal contamination in the high-K calc-alkaline and shoshonitic Neogene volcanic rocks of SE Spain. Lithos, 46, 773–802.

Bouroz, A., 1967. Correlations des tonsteins d'origine volcanique entre les bassins houillers de Sarre-Lorraine et du Nord-Pas-de-Calais. Comptes rendus hebdomadaires des séances de l'Académie des sciences, Série D, 264, 2729–2732.

Bronk Ramsey, C., 2008. Deposition models for chronological records. Quaternary Science Reviews, 27, 42–60.

Bronk Ramsey, C. & Lee, S., 2013. Recent and planned developments of the program OxCal. Radiocarbon, 55, 720–730.

Bruguier, O., Becq-Giraudon, J.F., Bosch, D. & Lancelot, J.R., 1998. Late Visean hidden basins in the internal zones of the Variscan belt: U-Pb zircon evidence from the French Massif Central. Geology, 26, 627–630.

Buhrke, V.E., Creasy, L.E., Croke, J.F., Feret, F., Jenkins, R., Kanare, H.M. & Kocman, V., 1998. Specimen preparation in X-Ray fluorescence. In Buhrke, V.E., Jenkins, R. & Smith, D.K. (eds), A Practical Guide for the Preparation of Specimens for X-Ray Fluorescence and X-Ray Diffraction Analysis. Wiley-VCH, New York, 59–122.

Bussy, F., Hernandez, J. & Von Raumer, J., 2000. Bimodal magmatism as a consequence of the post-collisional readjustment of the thickened Variscan continental lithosphere (Aiguilles Rouges-Mont Blanc Massifs, Western Alps). Transactions of the Royal Society of Edinburgh: Earth Sciences, 91, 221–233.

Chao, G.Y., 1969. 2θ (Cu) table for common minerals. Carleton University, Department of Geology, Geological Paper, 69–2, 42 p.

Chevalier, E. & Aretz, M., 2005. A microbe-bryozoan reef from the Middle Visean of the Namur Syncline (Engihoul quarry). Geologica Belgica, 8, 109–119.

Christidis, G.E., 1998. Comparative study of the mobility of major and trace elements during alteration of an andesite and a rhyolite to bentonite, in the islands of Milos and Kimolos, Aegean, Greece. Clays and Clay Minerals, 46, 379–399.

Christidis, G.E., Scott, P.W. & Marcopoulos, T., 1995. Origin of the bentonite deposits of eastern Milos, Aegean, Greece; geological, mineralogical and geochemical evidence. Clays and Clay Minerals, 43, 63–77.

Claiborne, L.L., Miller, C.F. & Wooden, J.L., 2010. Trace element composition of igneous zircon: a thermal and compositional record of the accumulation and evolution of a large silicic batholith, Spirit Mountain, Nevada. Contributions to Mineralogy and Petrology, 160, 511–531.

Clayton, T., Francis, J.E., Hillier, S.J., Hodson, F., Saunders, R.A. & Stone, J., 1996. The implications of reworking on the mineralogy and chemistry of Lower Carboniferous K-Bentonites. Clay Minerals, 31, 377–390.

Conil, R., Groessens, E., Laloux, M., Poty, E. & Tourneur, F., 1991. Carboniferous guide foraminifera, corals and conodonts in the Franco-Belgian and Campine Basins: their potential for widespread correlation. Courier Forschungsinstitut Senckenberg, 130, 15–30.

Coulon, M., Fourquin, C., Paicheler, J.C. & Point, R., 1975. Contribution à la connaissance du tectorogène varisque dans les Vosges méridionales. II—Le Culm de la région comprise entre Giromagny et Bourbach-le Bas. Sciences Géologiques: Bulletin, 28, 109–139.

Coulon, M., Fourquin, C. & Paicheler, J.C., 1979. Contribution à la connaissance du tectorogène varisque dans les Vosges méridionales, III-Le Culm entre Bourbach-le-Haut et le Molkenrain. Sciences Géologiques: Bulletin, 32, 117–129.

Dai, S., Wang, X., Zhou, Y., Hower, J.C., Li, D., Chen, W., Zhu, X. & Zou, J., 2011. Chemical and mineralogical compositions of silicic, mafic, and alkali tonsteins in the late Permian coals from the Songzao Coalfield, Chongqing, Southwest China. Chemical Geology, 282, 29–44.

Debon, F, D. & Lemmet, M., 1999. Evolution of Mg/Fe ratios in late Variscan plutonic rocks from the external crystalline massifs of the Alps (France, Italy, Switzerland). Journal of Petrology, 40, 1151–1185.

Delcambre, B., 1987. Application de la typologie du zircon à la téphrostratigraphie du Westphalien C de la Belgique et des régions limitrophes. Bulletin de la Société belge de Géologie, 96, 129–136.

Delcambre, B., 1989. Marqueurs téphrostratigraphiques au passage des calcaires de Neffe vers ceux de Lives. Bulletin de la Société Belge de Géologie, 98, 163–170.

Delcambre, B., 1996. Application de la typologie du zircon à la téphostratigraphie du Carbonifère de la Belgique et des régions limitrophes. Unpublished PhD thesis. Université Catholique de Louvain, Belgium, 318 p.

Delfour, J., 1989. Données lithostratigraphiques et géochimiques sur le Dévono-Dinantien de la partie sud du faisceau du Morvan (nord-est du Massif central français). Géologie de la France, 4, 49–77.

Devuyst, F.-X., Hance, L. & Poty, E., 2006. Moliniacian. Geologica Belgica, 9, 123–131.

Elder, W.P., 1988. Geometry of Upper Cretaceous bentonite beds: Implications about volcanic source areas and paleowind patterns, western interior, United States. Geology, 16, 835–838.

Fiebig, H.E.R., 1967. Das Namur C und Westfal im Niederrheinisch-Westfälischen Steinkohlengebiet. 6e Congrès International de Stratigraphie et de Géologie du Carbonifère, Sheffield, 79–89.

Finger, F., Roberts, M.P., Haunschmid, B., Schermaier, A. & Steyrer, H.P., 1997. Variscan granitoids of central Europe: their typology, potential sources and tectonothermal relations. Mineralogy and Petrology, 61, 67–96.

Floyd, P.A. & Winchester, J.A., 1978. Identification and discrimination of altered and metamorphosed volcanic rocks using immobile elements. Chemical Geology, 21, 291–306.

Gorton, M.P. & Schandl, E.S., 2000. From continents to island arcs: A geochemical index of tectonic setting for arc-related and within-plate felsic to intermediate volcanic rocks. The Canadian Mineralogist, 38, 1065–1073.

Govindaraju, K., 1994. 1994 compilation of working values and sample description for 383 geostandards. Geostandards Newsletter, 18, 1–158.

Güldenpfennig, M. & Loeschke, J., 1991. Petrographie und Geochemie unterkarbonischer Grauwacken und Vulkanite der Zone von Badenweiler-Lenzkirch in der Umgebung von Präg (Südschwarzwald). Jahreshefte Geologisches Landesamt Baden-Württemberg, 33, 5–32.

Han, G., Preat, A., Chamley, H., Deconinck, J.-F. & Mansy, J.-L., 2000. Palaeozoic clay mineral sedimentation and diagenesis in the Dinant and Avesnes Basins (Belgium, France): relationships with Variscan tectonism. Sedimentary Geology, 136, 217–238.

Hance, L., Devuyst, F.-X. & Poty, E., 2002. Sequence stratigraphy of the Belgian Lower Carboniferous - Tentative correlation with the British Isles. In Hills, L.V., Henderson, C.M. & Bamber, E.W. (eds), Carboniferous and Permian of the World. Canadian Society of Petroleum Geologists, Memoir. 19, 41–51.

Hance, L., Poty, E. & Devuyst, F.-X., 2006. Viséan. Geologica Belgica, 9, 55–62.

Helsen, S. & Kønigshof, P., 1994. Conodont thermal alteration patterns in Palaeozoic rocks from Belgium, northern France and western Germany. Geological Magazine, 131, 369–386.

Hill, I.G., Worden, R.H. & Meighan, I.G., 2000. Yttrium: The immobility-mobility transition during basaltic weathering. Geology, 28, 923–926.

Hoskin, P.W.O. & Schaltegger, U., 2003. The composition of zircon and igneous and metamorphic petrogenesis. Reviews in Mineralogy and Geochemistry, 53, 27–62.

Hoskin, P.W.O., Kinny, P.D., Wyborn, D. & Chappell, B.W., 2000. Identifying accessory mineral saturation during differentiation in granitoid magmas: an integrated approach. Journal of Petrology, 41, 1365–1396.

Huff, W.D., Merriman, R.J., Morgan, D.J. & Roberts, B., 1993. Distribution and tectonic setting of Ordovician K-bentonites in the United Kingdom. Geological Magazine, 130, 93–100.

Huff, W.D., Morgan, D.J. & Rundle, C.C., 1996. Silurian K-bentonites of the Welsh Borderlands : geochemistry, mineralogy and K-Ar ages of illitization. British Geological Survey, Technical Report WG/96/045, 25 p.

Imbrie, J., Berger, A., Boyle, E.A., Clemens, S.C., Duffy, A., Howard, W.R., Kukla, G., Kutzbach, J., Martinson, D.G., McIntyre, A., Mix, A.C., Molfino, B., Morley, J.J., Peterson, L.C., Pisias, N.G., Prell, W.L., Raymo, M.E., Shackleton, N.J. & Toggweiler, J.R., 1993. On the structure and origin of major glaciation cycles 2. The 100,000-year cycle. Paleoceanography, 8, 699–735.

Janoušek, V. & Gerdes, A., 2003. Timing the magmatic activity within the Central Bohemian Pluton, Czech Republic: conventional U-Pb ages for the Sázava and Tábor intrusions and their geotectonic significance. Journal of Geosciences, 48, 70–71.

Janoušek, V., Farrow, C.M. & Erban, V., 2006. Interpretation of whole-rock geochemical data in igneous geochemistry: Introducing Geochemical Data Toolkit (GCDkit). Journal of Petrology, 47, 1255–1259.

Jarvis, A., Reuter, H.I., Nelson, A. & Guevara, E., 2008. Hole-filled SRTM for the globe Version 4. Available from the CGIAR-CSI SRTM 90m Database. http://srtm.csi.cgiar.org, accessed 09/07/2017.

Kiipli, T., Soesoo, A., Kallaste, T. & Kiipli, E., 2008. Geochemistry of Telichian (Silurian) K-bentonites in Estonia and Latvia. Journal of Volcanology and Geothermal Research, 171, 45–58.

Klötzli, U.S. & Parrish, R.R., 1996. Zircon U/Pb and Pb/Pb geochronology of the Rastenberg granodiorite, South Bohemian Massif, Austria. Mineralogy and Petrology, 58, 197–214.

Königer, S., Lorenz, V., Stollhofen, H. & Armstrong, R., 2002. Origin, age and stratigraphic significance of distal fallout ash tuffs from the Carboniferous-Permian continental Saar-Nahe Basin (SW Germany). International Journal of Earth Sciences, 91, 341–356.

Kotková, J., Schaltegger, U. & Leichmann, J., 2010. Two types of ultrapotassic plutonic rocks in the Bohemian Massif — Coeval intrusions at different crustal levels. Lithos, 115, 163–176.

Kusiak, M.A., Dunkley, D.J., Suzuki, K., Kachlík, V., Kędzior, A., Lekki, J. & Opluštil, S., 2010. Chemical (non-isotopic) and isotopic dating of Phanerozoic zircon—A case study of durbachite from the Třebíč Pluton, Bohemian Massif. Gondwana Research, 17, 153–161.

Lakhrissi, M.A., 1996. Pétrologie, minéralogie, géochimie du volcanisme dévono-dinantien des Vosges méridionales (France). Unpublished PhD thesis. Université des Sciences et Technologies de Lille, France, 414 p.

Lardeaux, J.M., Schulmann, K., Faure, M., Janousek, V., Lexa, O., Skrzypek, E., Edel, J.B. & Stípská, P., 2014. The Moldanubian Zone in the French Massif Central, Vosges/Schwarzwald and Bohemian Massif revisited: differences and similarities. Geological Society, London, Special Publications, 405, 7–44.

Laurent, O., Couzinié, S., Zeh, A., Vanderhaeghe, O., Moyen, J.-F., Villaros, A., Gardien, V. & Chelle-Michou, C., 2017. Protracted, coeval crust and mantle melting during Variscan late-orogenic evolution: U–Pb dating in the eastern French Massif Central. International Journal of Earth Sciences, 106, 421–451.

Lefevre, C., Lakhrissi, M. & Schneider, J.-L., 1994. Les affinités magmatiques du volcanisme dinantien des Vosges méridionales (France); approche géochimique et interprétation. Comptes rendus de l'Académie des sciences. Série 2. Sciences de la terre et des planètes, 319, 79–86.

Li, C., Arndt, N.T., Tang, Q. & Ripley, E.M., 2015. Trace element indiscrimination diagrams. Lithos, 232, 76–83.

McCann, T., Skompski, S., Poty, E., Dusar, M., Vozárová, A., Schneider, J., Wetzel, A., Krainer, K., Kornpihl, K., Schäefer, A., Krings, M., Oplustil, S. & Tait, J., 2006. Carboniferous. In McCann, T. (ed.), The Geology of Central Europe: Volume 1, Precambrian and Palaeozoic. Geological Society, London, 411–529.

McDonough, W.F. & Sun, S. -s., 1995. The composition of the Earth. Chemical Geology, 120, 223–253.

Merriman, R.J. & Roberts, B., 1990. Metabentonites in the Moffat Shale Group, Southern Uplands of Scotland: Geochemical evidence of ensialic marginal basin volcanism. Geological Magazine, 127, 259–271.

Monaghan, A.A. & Parrish, R.R., 2006. Geochronology of Carboniferous–Permian magmatism in the Midland Valley of Scotland: implications for regional tectonomagmatic evolution and the numerical time scale. Journal of the Geological Society, 163, 15–28.

Paproth, E., Conil, R., Bless, M.J.M., Boonen, P., Bouckaert, J., Carpentier, N., Coen, M., Delcambre, B., Deprijck, C., Deuzon, S., Dreesen, R., Groessens, E., Hance, L., Hennebert, M., Hibo, D., Hahn, G., Hahn, R., Hislaire, O., Kasig, W., Laloux, M., Lauwers, A.S., Lees, A., Lys, M., Op de beek, K., Overlau, P., Pirlet, H., Poty, E., Ramsbottom, W., Streel, M., Swennen, R., Thorez, J., Vanguestaine, M., Van Steenwinkel, M. & Vieslet, J.-L., 1983. Bio- and lithostratigraphic subdivisions of the Dinantian in Belgium, a review. Annales de la Société Géologique de Belgique, 106, 185–239.

Pearce, J.A., 1982. Trace element characteristics of lavas from destructive plate boundaries. In Thorpe, R.S. (ed.), Orogenic Andesites and Related Rocks. John Wiley and Sons, Chichester, England, 528–548.

Pearce, J.A., 2014. Geochemical fingerprinting of the Earth's oldest rocks. Geology, 42, 175–176.

Pearce, J.A. & Peate, D.W., 1995. Tectonic implications of the composition of volcanic arc magmas. Annual Review of Earth and Planetary Sciences, 23, 251–285.

Pearce, J.A., Harris, N.B.W. & Tindle, A.G., 1984. Trace element discrimination diagrams for the tectonic interpretation of granitic rocks. Journal of Petrology, 25, 956–983.

Pirlet, H., 1963. Sédimentologie des formations du Viséen supérieur, V3b dans la Vallée du Samson (Bassin de Namur, Belgique). Annales de la Société Géologique de Belgique, 86, M3–M41.

Pirlet, H., 1968. La sédimentation rythmique et la stratigraphie du Viséen supérieur V3b, V3c inférieur dans les synclinoriums de Namur et de Dinant. Académie royale de Belgique, Classe des Sciences, Mémoires in-4°, 2e série, 17, 7–98.

Pointon, M.A., 2012. Constraining global Carboniferous climatic fluctuations using high resolution geochronology. Unpublished PhD thesis. University of Dublin, Trinity College, Ireland, 345 p.

Pointon, M.A., Chew, D.M., Ovtcharova, M., Sevastopulo, G.D. & Crowley, Q.G., 2012. New high-precision U-Pb dates from western European Carboniferous tuffs; implications for time scale calibration, the periodicity of late Carboniferous cycles and stratigraphical correlation. Journal of the Geological Society, 169, 713–721.

Pointon, M.A., Chew, D.M., Ovtcharova, M., Sevastopulo, G.D. & Delcambre, B., 2014. High-precision U-Pb zircon CA-ID-TIMS dates from western European late Visean bentonites. Journal of the Geological Society, 171, 649–658.

Poty, E., 2016. The Dinantian (Mississippian) succession of southern Belgium and surrounding areas: stratigraphy improvement and inferred climate reconstruction. Geologica Belgica, 19, 177–200.

Poty, E. & Hance, L., 2006a. Livian. Geologica Belgica, 9, 133–138.

Poty, E. & Hance, L., 2006b. Warnantian. Geologica Belgica, 9, 139–144.

Poty, E., Hance, L., Lees, A. & Hennebert, M., 2001. Dinantian lithostratigraphic units (Belgium). Geologica Belgica, 4, 69–93.

Poty, E., Devuyst, F.-X. & Hance, L., 2006. Upper Devonian and Mississippian foraminiferal and rugose coral zonations of Belgium and northern France: a tool for Eurasian correlations. Geological Magazine, 143, 829–857.

Pupin, J.P., 1980. Zircon and granite petrology. Contributions to Mineralogy and Petrology, 73, 207–220.

Rubatto, D., Schaltegger, U., Lombardo, B. & Compagnoni, R., 2001. Complex Paleozoic magmatic and metamorphic evolution in the Argentera Massif (Western Alps) resolved with U-Pb dating. Schweizerische Mineralogische und Petrographische Mitteilungen, 81, 213–228.

Rudnick, R.L. & Gao, S., 2003. Composition of the continental crust. In Holland, H.D. & Turekian, K.K. (eds), Treatise on Geochemistry, Vol. 3. Pergamon, Oxford, 1–64.

Schaltegger, U., 1997. Magma pulses in the Central Variscan Belt: episodic melt generation and emplacement during lithospheric thinning. Terra Nova, 9, 242–245.

Schaltegger, U., 2000. U-Pb geochronology of the Southern Black Forest Batholith (Central Variscan Belt): timing of exhumation and granite emplacement. International Journal of Earth Sciences, 88, 814–828.

Schaltegger, U. & Corfu, F., 1992. The age and source of late Hercynian magmatism in the central Alps: evidence from precise U−Pb ages and initial Hf isotopes. Contributions to Mineralogy and Petrology, 111, 329–344.

Schaltegger, U., Schneider, J.-L., Maurin, J.-C. & Corfu, F., 1996. Precise U–Pb chronometry of 345–340 Ma old magmatism related to syn-convergence extension in the Southern Vosges (Central Variscan Belt). Earth and Planetary Science Letters, 144, 403–419.

Schandl, E.S. & Gorton, M.P., 2002. Application of high field strength elements to discriminate tectonic settings in VMS environments. Economic Geology, 97, 629–642.

Schneider, P.J.-L., Maass, R., Gall, J.-C. & Duringer, P., 1989. L'événement intraviséen dans la zone moldanubienne de la chaîne varisque d'Europe: les données des formations volcano-sédimentaires dévono-dinantiennes du Massif Central Français, des Vosges du Sud (France) et de la Forêt Noire (R.F.A.). Geologische Rundschau, 78, 555–570.

Schoene, B., Crowley, J.L., Condon, D.J., Schmitz, M.D. & Bowring, S.A., 2006. Reassessing the uranium decay constants for geochronology using ID-TIMS U–Pb data. Geochimica et Cosmochimica Acta, 70, 426–445.

Schulmann, K., Schaltegger, U., Jezek, J., Thompson, A.B. & Edel, J.-B., 2002. Rapid burial and exhumation during orogeny: Thickening and synconvergent exhumation of thermally weakened and thinned crust (Variscan orogen in Western Europe). American Journal of Science, 302, 856–879.

Sevastopulo, G.D. & Barham, M., 2014. Correlation of the base of the Serpukhovian Stage (Mississippian) in NW Europe. Geological Magazine, 151, 244–253.

Snow, C.A., 2006. A reevaluation of tectonic discrimination diagrams and a new probabilistic approach using large geochemical databases: Moving beyond binary and ternary plots. Journal of Geophysical Research: Solid Earth, 111, B06206.

Somerville, I.D., Strogen, P. & Jones, G.L., 1992. Biostratigraphy of Dinantian limestones and associated volcanic rocks in the Limerick Syncline, Ireland. Geological Journal, 27, 201–220.

Spears, D.A., 2006. Clay mineralogy of onshore UK Carboniferous mudrocks. Clay Minerals, 41, 395–416.

Spears, D.A. & Kanaris-Sotiriou, R., 1979. A geochemical and mineralogical investigation of some British and other European tonsteins. Sedimentology, 26, 407–425.

Spears, D.A. & O'Brien, P.J., 1994. Origin of British tonsteins and tectonomagmatic implications. Zentralblatt für Geologie und Paläontologie, Teil I, 5/6, 491–497.

Spears, D.A. & Lyons, P.C., 1995. An update on British tonsteins. Geological Society, London, Special Publications, 82, 137–146.

Spears, D.A., Kanaris-Sotiriou, R., Riley, N. & Krause, P., 1999. Namurian bentonites in the Pennine Basin, UK - origin and magmatic affinities. Sedimentology, 46, 385–401.

Stephenson, D., Goodenough, K.M., Loughlin, S.C., Millward, D. & Waters, C.N., 2003. Carboniferous and Permian igneous rocks of Great Britain, north of the Variscan Front: an introduction. In Stephenson, D., Loughlin, S.C., Millward, D., Waters, C.N. & Williamson, I.T. (eds), Carboniferous and Permian Igneous Rocks of Great Britain North of the Variscan Front. Geological Conservation Review Series, 27, 3–34.

Strogen, P., 1988. The Carboniferous lithostratigraphy of Southeast County Limerick, Ireland, and the origin of the Shannon Trough. Geological Journal, 23, 121–137.

Sun, S. -s. & McDonough, W.F., 1989. Chemical and isotopic systematics of oceanic basalts: implications for mantle composition and processes. Geological Society, London, Special Publications, 42, 313–345.

Sverjensky, D.A., 1984. Europium redox equilibria in aqueous solution. Earth and Planetary Science Letters, 67, 70–78.

Tabaud, A.-S., Janoušek, V., Skrzypek, E., Schulmann, K., Rossi, P., Whitechurch, H., Guerrot, C. & Paquette, J.-L., 2014. Chronology, petrogenesis and heat sources for successive Carboniferous magmatic events in the Southern–Central Variscan Vosges Mts (NE France). Journal of the Geological Society, 172, 87–102.

Thompson, R.N., Dickin, A.P., Gibson, I.L. & Morrison, M.A., 1982. Elemental fingerprints of isotopic contamination of hebridean Palaeocene mantle-derived magmas by Archaean sial. Contributions to Mineralogy and Petrology, 79, 159–168.

Thorez, J. & Pirlet, H., 1979. Petrology of K-bentonite beds in the carbonate series of the Visean and Tournaisian stages of Belgium. In Mortland, M.M. & Farmer, V.C. (eds), Proceedings of the 6th International Clay Conference held in Oxford, 10-14 July, 1978. Developments in Sedimentology, 27, Elsevier, Amsterdam, 323–332.

Timmerman, M.J., 2004. Timing, geodynamic setting and character of Permo-Carboniferous magmatism in the foreland of the Variscan Orogen, NW Europe. Geological Society, London, Special Publications, 223, 41–74.

Trail, D., Bruce Watson, E. & Tailby, N.D., 2012. Ce and Eu anomalies in zircon as proxies for the oxidation state of magmas. Geochimica et Cosmochimica Acta, 97, 70–87.

Turner, S., Arnaud, N., Liu, J., Rogers, N., Hawkesworth, C., Harris, N., Kelley, S., Van Calsteren, P. & Deng, W., 1996. Post-collision, shoshonitic volcanism on the Tibetan Plateau: Implications for convective thinning of the lithosphere and the source of ocean island basalts. Journal of Petrology, 37, 45–71.

von Raumer, J.F., Finger, F., Veselá, P. & Stampfli, G.M., 2014. Durbachites-Vaugnerites - a geodynamic marker in the central European Variscan orogen. Terra Nova, 26, 85–95.

Walker, G.P.L., 1971. Grain-size characteristics of pyroclastic deposits. Journal of Geology, 79, 696–714.

Wang, P. & Glover, L., 1992. A tectonics test of the most commonly used geochemical discriminant diagrams and patterns. Earth-Science Reviews, 33, 111–131.

Wark, D.A. & Miller, C.F., 1993. Accessory mineral behavior during differentiation of a granite suite: monazite, xenotime and zircon in the Sweetwater Wash pluton, southeastern California, U.S.A. Chemical Geology, 110, 49–67.

Waters, C.N. & Condon, D.J., 2012. Nature and timing of Late Mississippian to Mid-Pennsylvanian glacio-eustatic sea-level changes of the Pennine Basin, UK. Journal of the Geological Society, 169, 37–51.

Weaver, C.E., 1963. Interpretative value of heavy minerals from bentonites. Journal of Sedimentary Research, 33, 343–349.

Wilson, L. & Walker, G.P.L., 1987. Explosive volcanic eruptions - VI. Ejecta dispersal in plinian eruptions: the control of eruption conditions and atmospheric properties. Geophysical Journal International, 89, 657–679.

Winchester, J.A. & Floyd, P.A., 1977. Geochemical discrimination of different magma series and their differentiation products using immobile elements. Chemical Geology, 20, 325–343.

Wray, D.S., 1995. Origin of clay-rich beds in Turonian chalks from Lower Saxony, Germany — A rare-earth element study. Chemical Geology, 119, 161–173.

Wray, D.S. & Wood, C.J., 1998. Distinction between detrital and volcanogenic clay-rich beds in Turonian–Coniacian chalks of eastern England. Proceedings of the Yorkshire Geological Society, 52, 95–105.

Zachovalová, K. & Leichmann, J., 2003. Clasts of volcanic rocks from the Visean conglomerates in the Drahany Culm: evidence for a volcanic arc on the eastern margin of Bohemian Massif. Journal of the Czech Geological Society, 48, 139.

Zielinski, R., 1982. The mobility of uranium and other elements during alteration of rhyolite ash to montmorillonite: A case study in the Troublesome Formation, Colorado, U.S.A. Chemical Geology, 35, 185–204.

Manuscript received 20.09.2016, accepted in revised form 06.11.2017, available on line 14.02.2018.